NUCLEAR STRUCTURE EFFECTS IN INTERNAL CONVERSION

Thesis by

Edwin Charles Seltzer

In Partial Fulfillment of the Requirements

For the Degree of

Doctor of Philosophy

California Institute of Technology

Pasadena, California

1966

(Submitted October 13, 1965)

ACKNOWLEDGEMENTS

The author would like to thank: Professor F. Boehm, for his interest and support. Dr. E. Kankeleit, for his time and interest in the completion of this thesis. R. Hager, who collaborated with the author in all phases of a program of investigating internal conversion effects. H. Hendrickson and R. Marcley for their support in problems involving experimental equipment. Dr. R. Brockmeier, for many discussions concerning programming for digital computers.

ABSTRACT

Experimental studies of nuclear effects in internal conversion in Ta^{181} and Lu^{175} have been performed. Nuclear structure effects ("penetration" effects), in internal conversion are described in general. Calculations of theoretical conversion coefficients are outlined. Comparisons with the theoretical conversion coefficient tables of Rose and Sliv and Band are made. Discrepancies between our results and those of Rose and Sliv are noted. The theoretical conversion coefficients of Sliv and Band are in substantially better agreement with our results than are those of Rose. The ratio of the M1 penetration matrix element to the M1 gamma-ray matrix element, called λ, is equal to $+ 175 \pm 25$ for the 482 keV transition in Ta^{181}. The results for the 343 keV transition in Lu^{175} indicate that λ may be as large as $- 8 \pm 5$. These transitions are discussed in terms of the unified collective model. Precision L subshell measurements in Tm^{169} (130 keV), W^{182} (100 keV), and Ta^{181} (133 keV) show definite systematic deviations from the theoretical conversion coefficients. The possibility of explaining these deviations by penetration effects is investigated and is shown to be excluded. Other explanations of these anomalies are discussed.

TABLE OF CONTENTS

		Page
ACKNOWLEDGEMENTS		ii
ABSTRACT		iii
CHAPTER		
I	Introduction	1
II	Theoretical Conversion Coefficients	9
	A. Derivation of Formulae B. Numerical Calculation of Conversion Coefficients C. Comparison with Previous Calculations	
III	General Aspects of Internal Conversion Involving Penetration Effects	22
	A. Form of the Operators B. Nuclear Model C. Characteristics of Electric Transitions	
IV	Experimental Technique	30
	A. Magnetic Spectrometer B. Detectors C. Source Preparation D. Data Collection	
V	Experiments	37
	A. Results for Magnetic Dipole Cases B. Comparison of Results with Nuclear Model Calculations C. Anomalies in Electric Quadrupole Internal Conversion in the L Shell D. Estimation of Penetration Effects E. Other Possible Causes of E2 Anomalies	
VI	Conclusions	66
APPENDICES		
I	Notation and Formulae	69
II	Conversion Coefficient Formulae	72
REFERENCES		75

I. INTRODUCTION

The de-excitation of the excited states of nuclei can occur in many ways. The most prominent process for states below the heavy particle emission threshold is gamma-ray emission. There are two other electromagnetic decay modes that are associated with gamma-ray emission. Internal pair emission with a threshold of 2m (where m is the electron mass) can be considered a high-energy process. While its rate is only 10^{-4} times that of gamma-ray emission, internal pair formation is of interest as a sensitive means of determining the multi-polarity of the transitions[1].

A much more frequently studied process is that of internal conversion. This decay mode occurs through the interaction of the nuclear current with that of one of the atomic electrons, usually an inner one, producing a free electron with an energy equal to the transition energy minus the electron binding energy. This process is much more probable than gamma-ray emission at sufficiently low transition energies. Customarily, interest in internal conversion is twofold: 1) the excellent energy resolution of magnetic spectrometers and, 2) the sensitivity to the transition multipolarity up to moderate energies (less than 1 MeV).

If the nuclear transition is between spin zero states, then gamma-ray emission is forbidden and internal conversion and internal pair formation are the dominant decay modes. Two-photon emission is possible, but has never been observed. Internal conversion in the $J = 0 \rightarrow J = 0$, no parity change transition, the "electric monopole"

transition, is interesting as it can only proceed by interaction of the nuclear charge with the electron when it is inside the nucleus[2]. Electric monopole transitions cal also occur in transitions between states of the same non-zero spin and parity, but then other multipolarities are dominant. The unusual nature of the electric monopole transitions suggested to Church and Weneser that "penetration" effects may be significant in the internal conversion of the other multipole radiations[3]. The occurence of different types of nuclear matrix elements in the penetration amplitudes was noted. We shall be especially interested in these penetration effects.

If one neglects the finite size of the nucleus, it is possible to express the probability for internal conversion as a product of a term representing the rate of gamma emission and a term which depends solely on the atomic electron wave functions. This latter quantity is called the internal conversion coefficient. It is a function of the transition energy, atomic number, and transition multipolarity. Early attempts to calculate internal conversion coefficients assumed the process was similar to the photoelectric effect[4,5]. It was soon recognized that a second order process was involved, akin to the Auger effect. That is, a direct interaction of the nuclear and electron currents[6]. Not yet realizing that nuclear gamma emissions were not always E1 in character, there was considerable confusion interpreting the early experiments[7-10]. There was even an improbable E0 transition included among the first few conversion

lines examined.

The early calculations were based upon unscreened Dirac wave functions. The rapid variation of conversion coefficients with atomic number and transition energy requires extensive tabulations if their remarkable properties are to be of use in determining nuclear structures. Major calculational efforts were first made by M.E. Rose and co-workers using unscreened point Coulomb wave functions[11,12]. Screening was shown by Reitz to have only a moderate influence[13].

The finite size of the nucleus was shown by Sliv to have a large effect, especially for magnetic multipoles[14,15]. The singularity of the Coulomb field introduces a weak integrable singularity into the Dirac wave functions. The effect on the conversion coefficients may be as large as 50% for M1 transitions in heavy nuclei. A Coulomb potential modified for the effects of finite nuclear size gives conversion coefficients which are relatively insensitive to the details of the cut-off[16].

We have already mentioned the altered form of the interaction for electrons penetrating the nucleus (e.g., in E0 transitions). Additional contributions of this sort were emphasized by Church and Weneser[3]. These additional contributions do not have the property of factoring into a nuclear term and an atomic term. Their calculation is dependent upon knowledge of the nuclear wave function. Church and Weneser showed that if the normal gamma-ray transition amplitude was hindered due to a nuclear selection rule effect, then the "penetration" terms may be unhindered. Therefore, if the normal

gamma-ray transition amplitude is hindered sufficiently, the penetration amplitude may be large enough to observe in spite of the small probability of the electron being inside the nucleus. The experiments that will be described in this thesis are concerned with these effects.

All the many experimental techniques of low-energy nuclear physics are concerned with measuring nuclear matrix elements. The nuclear matrix element usually involves the electromagnetic and beta interactions. However, measurements of the energy level spectrum give information about the nuclear interaction when considered in the context of a particular nuclear model. The theory of the beta interaction involves a number of possible matrix elements, which, in general, are hard to determine. Absolute decay rate measurements give their magnitude; and measurements of the electron energy spectrum, and, if possible, beta-gamma directional and beta-gamma circular polarization correlations give their ratios. In the case of electromagnetic interactions there are fewer matrix elements involved. Also there is the possibility of measuring diagonal matrix elements, such as, the electric quadrupole and magnetic dipole moments. The electromagnetic interaction of the nucleus with atomic electrons has the additional feature of an "internal" field perturbing the nucleus, the "penetration" contribution.

Penetration effects occur in cases other than internal conversion. The isotope shift seen in optical or x-ray spectra is a finite nuclear size effect related to the relative change

in the nuclear charge distributions of two isotopes. The isomer shift seen in Mössbauer spectra measures the change in the nuclear charge distributions for two levels in the same isotope. There is a magnetic dipole "anomaly" also. If one measures the magnetic dipole moment of a nucleus with both NMR and atomic beam studies of the magnetic hyperfine interaction, one finds a small difference. The atomic hyperfine interaction contains a penetration contribution which gives further information about the distribution of nuclear magnetism. Penetration effects are seen in high-energy electron scattering. This is the best method for determining the charge distribution of the nucleus. Inelastic electron scattering is also expected to yield information about the nuclear current distribution.

Penetration effects associated with internal conversion are especially noteworthy. Since they compete with the normal transition amplitudes, which may be hindered, it is possible to find cases where internal conversion is dominated by the penetration amplitude. This is unlikely for magnetic dipole "anomalies", where the main contribution is a diagonal matrix element, not expected to be hindered. The analysis of penetration effects in internal conversion is straightforward in principle because only inner electron shells are involved. The problem of finding suitable wave functions and calculating the normal conversion amplitudes is solved in this thesis. The possibility of finding additional nuclear matrix elements for retarded transitions can be an aid in trying to understand the cause of the retardation. Two retarded M1 transitions in Lu^{175} and Ta^{181} are studied in this thesis. The case in Ta^{181} is the most highly

retarded M1 transition known.

Electric gamma-ray transition amplitudes are expected to be described by the long-wavelength limit approximation (Siegert's Theorem). The higher order contributions cannot be seen since they are proportional to the ratio of the nuclear radius to photon wavelength. In the case of an atomic electron probing the nucleus, the wavelength of a 15 - 30 MeV electron at the nucleus is comparable to nuclear dimensions. For the first time these additional terms may be seen in nuclear electric multipole transitions. As will be discussed, they have different properties under time reversal and so are affected differently by nuclear pairing correlations than is the normal amplitude. The spin current will be seen to be able to make a large contribution to the electric multipole transition amplitude. Several cases of electric quadrupole transitions are studied in an effort to find precisely what, if any, anomalies they may have for internal conversion. The possibility of anomalies in E2 conversion has been often raised.

The two tabulations of Sliv[16] and Rose[17] took account of penetration effects in different ways. Rose argues that since these nuclear structure effects can be observed only in the exceptional case, deserving individual analysis, and are small in the ordinary case, one could disregard them altogether. Sliv included their effect in his tabulated values by using a dimensional estimate of their magnitude, a kind of "Weisskopf estimate". The penetration effects increase relative to the normal conversion process with an increase in atomic number and transition energy[18]. Generally, the

estimate of Sliv, the so-called "surface current model", is understood to be of the order of a few percent of the usual conversion coefficient. However, in connection with our own calculations we investigated the "surface current" estimate and found contributions as large as 10% for large Z.

Both Rose and Sliv claim their calculations are accurate and should agree with experiment to within a few percent, say 5%. They assume, of course, that nuclear structure effects are no larger than dimensional estimates. Experimentalists have generally believed this, attributing discrepancies to nuclear structure effects or more honestly to systematic errors. Recently, the problem of the accuracy of the calculated conversion coefficients has interested a number of people. Listengarten has reviewed conversion coefficient experiments up to 1961, finding that those experiments which are most reliable agree excellently with the tabulated values[19,20]. Unfortunately, these few precise experiments involve for the most part E2 K shell conversion at the moderately high energies of 300 to 400 keV. It is also to be mentioned that the tabulations of Rose and Sliv agree to within a few percent in the K shell, especially for E2 conversion. Still, it was concluded that as experimental techniques were refined the tabulated values would prove to be accurate to a few percent for K conversion and probably for L shell conversion also . In 1964 Novakov and Hollander, analyzing very careful measurements of L subshell conversion ratios, made the observation that Rose and Sliv's values do not agree very well for L subshell conversion[21]. The

discrepancy was sometimes as large as 50% for M1 transitions. The L shell theoretical ratios (L_I/L_{II} and L_{II}/L_{III}) of Sliv and Rose are actually in better agreement, and can be used to analyze for E2/M1 mixing. The small inconsistencies which they found in the E2/M1 mixing, derived from the L_I/L_{III} and L_{II}/L_{III} ratios, seemed now to be attributable to the theoretical conversion coefficients.

Since we planned to undertake L subshell ratio measurements in order to determine nuclear structure effects, it had been planned to recalculate the internal conversion coefficients in order to have the requisite theoretical results available for analyzing our experiments. The observations of Novakov and Hollander raised the question whether the calculated theoretical values contained numerical errors. If this is the case, then new calculations are of interest in addition to their usefulness in analyzing our experiments.

II. THEORETICAL CONVERSION COEFFICIENTS

A. Derivation of Formulae

The starting point for internal conversion calculations is the retarded interaction between the nuclear and electron currents:[22]

$$H = - \int dV_e dV_n \; (\vec{j}_n \cdot \vec{j}_e - \rho_n \rho_e) \; \frac{e^{iKR}}{R} \tag{1}$$

where $R = |\vec{r}_n - \vec{r}_e|$ and K is the nuclear transition energy $E_i - E_f$. A more useful form for calculation is obtained by means of expansion

$$\frac{e^{iKR}}{R} = 4\pi iK \sum_{L,M} Y_L^{m*} (\Omega_x) \; Y_L^m (\Omega_y) \; x \begin{cases} j_L(Kx) \; h_L^{(1)}(Ky) & y > x \\ h_L^{(1)}(Kx) \; j_L(Ky) & y < x \end{cases} \tag{2}$$

and the expansion of the electromagnetic potentials in eigenfunctions of angular momentum

$$\vec{A}_L^m (M) = - j_L(Kx) \; \vec{T}_{L,L}^{\,m}$$

$$\vec{A}_L^m (e) = \left(\frac{L+1}{2L+1}\right)^{1/2} j_{L-1} (Kx) \; \vec{T}_{L,L-1}^{\,m} - \left(\frac{L}{2L+1}\right)^{1/2} j_{L+1}(Kx) \; \vec{T}_{L,L+1}^{\,m}$$

$$\vec{A}_L^m (\ell) = \left(\frac{L}{2L+1}\right)^{1/2} j_{L-1} (Kx) \; \vec{T}_{L,L-1}^{\,m} + \left(\frac{L+1}{2L+1}\right)^{1/2} j_{L+1} (Kx) \; \vec{T}_{L,L+1}^{\,m} \tag{3}$$

The $\vec{T}_{\mu,\lambda}^{\,m}$ are the usual vector spherical harmonics[23]. Equation (1) then becomes for the L^{th} magnetic and electric multipole

$$\begin{aligned} \frac{-H_L^m (M)}{(4\pi iK)} = & \int_{V_n} dV_n \; \vec{j}_n \cdot \vec{B}_L^{m*}(M) \int_0^{r_n} dV_e \; \vec{j}_e \cdot \vec{A}_L^m (M) \\ & + \int_{V_n} dV_n \; \vec{j}_n \cdot \vec{A}_L^{m*}(M) \int_{r_n}^{\infty} dV_e \; \vec{j}_e \cdot \vec{B}_L^m (M) \end{aligned} \tag{4}$$

and

$$\frac{-H_L^m(e)}{(4\pi iK)} = \int dV_n\ \vec{j}_n \cdot \vec{B}_L^{m*}(e) \int_0^{r_n} dV_e\ \vec{j}_e \cdot \vec{A}_L^m(e) + \int dV_n\ \vec{j}_n \cdot \vec{A}_L^{m*}(e) \cdot \int_{r_n}^{\infty} dV_e\ \vec{j}_e \cdot \vec{B}_L^m(e)$$

$$+ \int dV_n\ \vec{j}_n \cdot \vec{B}_L^{*m}(\ell) \int_0^{r_n} dV_e\ \vec{j}_e \cdot \vec{A}_L^m(\ell) + \int dV_n\ \vec{j}_n \cdot \vec{A}_L^{*m}(\ell) \cdot \int_{r_n}^{\infty} dV_e\ \vec{j}_e \cdot \vec{B}_L^m(\ell) \qquad (5)$$

$$- \int dV_n \rho_n\ Y_L^{m*}\ h_L^{(1)}(Kr_n) \int_0^{r_n} dV_e \rho_e\ Y_L^m\ j_L(Kr_e)$$

$$- \int dV_n \rho_n\ Y_L^{m*}\ j_L(Kr_n) \int_{r_n}^{\infty} dV_e \rho_e\ Y_L^m\ h_L^{(1)}(Kr_e).$$

The $\vec{B}_L^m$ are defined to be the same as the $\vec{A}_L^m$, Eq. (3), with j_L replaced by $h_L^{(1)}$. Equations (4) and (5) follow from time-dependent perturbation theory[24,25]. The details of the reduction of Eqs. (4) and (5) are given in Appendix II. The procedure for the magnetic multipoles, which is straightforward, will be outlined here in order to illustrate some of the statements made before. First, Eq. (4) is rewritten

$$\frac{-H_L^m(M)}{(4\pi iK)} = \int dV_n\ \vec{j}_n \cdot \vec{A}_L^{*m}(M) \int_0^{\infty} dV_e\ \vec{j}_e \cdot \vec{B}_L^m(M)$$

$$+ \int dV_n\ \vec{j}_n \cdot \left\{ \vec{B}_L^{m*}(M) \int_0^{r_n} dV_e\ \vec{j}_e \cdot \vec{A}_L^m(M) - \vec{A}_L^{*m}(M) \int_0^{r_n} dV_e\ \vec{j}_e \cdot \vec{B}_L^m(M) \right\} . \qquad (6)$$

We now perform the integrations over the electron angles

$$\frac{-H_L^m(M)}{(4\pi iK)} = A\left[\int dV_n\ \vec{j}_n\cdot\vec{A}_L^{m*}(M)\int_0^\infty dr_e(g_f f_i + f_f g_i)\ h_L^{(1)}(Kr_e)\right.$$
$$+\int dV_n\ \vec{j}_n\cdot\left\{\vec{B}_L^{m*}(M)\int_0^{r_n} dr_e(g_f f_i + f_f g_i)\ j_L(Kr_e)\right. \qquad (7)$$
$$\left.\left. - A_L^{m*}(M)\int_0^{r_n} dr_e(g_f f_i + f_f g_i)\ h_L^{(1)}(Kr_e)\right\}\right] \quad .$$

(See Appendix I for notation).

A is a term that represents the angular integration. Equation (7) now demonstrates the fact that the amplitude for internal conversion is the sum of two terms. The first term is proportional to the amplitude for gamma-ray emission times a completely calculable factor depending only on the atomic wavefunctions. The square of this factor summed over all partial waves allowed by the transition multipolarity directly yields the conversion coefficient. We shall henceforth refer to this factor as a "radial integral". The second term does not factor into nuclear and electronic terms, has a nuclear interaction which is different from that of gamma-ray emission, and is proportional to the amplitude for an electron to be inside the nucleus.

In order to make a few simple points, we shall write some formal expressions. Let us represent the amplitudes for gamma-ray emission and internal conversion as M_γ and M_e, respectively. Now the rate of conversion can be written,

$$N_e = \sum_\kappa C_\kappa\ |M_e|_\kappa^2 \qquad (8)$$

$$= \sum_\kappa C_\kappa\ |M_\gamma|^2 |R_\kappa + \frac{M_p}{M_\gamma}\ \Delta R_\kappa|^2 \qquad (9)$$

where κ indexes the final states, R_κ is the radial integral, M_p is the nuclear vertex for interaction with the penetrating electron, and ΔR_κ is an electron weighting factor. Writing $\lambda = M_p/M_\gamma$ we can define the conversion coefficient,

$$\alpha \equiv \frac{N_e}{N_\gamma} = \sum_\kappa C_\kappa \left| R_\kappa + \lambda \, \Delta R_\kappa \right|^2 . \tag{10}$$

If the gamma-ray transition is hindered and the penetration contribution is not, then λ may be a large number. In this case, the measured conversion coefficient is markedly different from the "book" coefficient:

$$\bar{\alpha} \equiv \sum_\kappa C_\kappa \left| R_\kappa \right|^2 . \tag{11}$$

Actually, Eq. (11) is the theoretical coefficient that Rose used; but Sliv, as we said before, used the dimensional estimate $\lambda \equiv 1$ in Eq. (10) for his theoretical coefficient. It is clear from Eq. (10) that since the penetration contribution is coherent with the main conversion term, it does not suffice to know only conversion coefficients to analyze situations where "penetration" occurs. One needs all the radial integrals R_κ and the weighting factors ΔR_κ. In fact, Eq. (10) must be generalized; the penetration term in Eq. (7) can be expanded using the power series expressions for the bound and continuum wave functions, as well as for the Bessel functions. Therefore,

$$\lambda \Delta R_\kappa \rightarrow \sum_n \frac{\Delta R_\kappa^{(n)}}{M_\gamma} \int \vec{j}_n \cdot \vec{A}_L^m \, r^n \, dV_n \tag{12}$$

or

$$\lambda \, \Delta R_{\kappa} \rightarrow \sum_{n} \lambda^{(n)} \Delta R_{\kappa}^{(n)} \quad . \tag{13}$$

The $\lambda^{(n)}$ are now defined in such a way that for a given transition, they are the same for all final states as well as for all electron shells. While, of course, approximations may be expected, a single determination of a conversion coefficient cannot determine even a dominant λ. This is precluded by the quadratic nature of the expression for an intensity.

There are two ways to resolve this problem. An angular correlation involving a conversion electron can, if enough is known about the other radiations, determine the phase of λ from the interference of the various electron partial waves. Or one can over-determine the λ's experimentally and look for consistent solutions. While one usually attempts to do this in order to increase the reliability of the analysis, it is not necessary for the different data to be "orthogonal" in the sense of each measurement containing new information. In these cases one can try using a nuclear model to distinguish between very different solutions.

B. Numerical Calculation of Conversion Coefficients

The numerical problems involved in calculating conversion coefficients may be summarized:

1. Choice of electron potential
2. Choice of nuclear charge distribution
3. Starting solution at origin and infinity
4. Method of integration of Dirac equation

5. Finding eigenvalue
6. Normalization of continuum solution
7. Generation of Bessel functions
8. Computation of radial integrals.

Both Rose and Sliv used the Thomas-Fermi-Dirac potential tabulations in the literature[27-29]. The T-F-D potential includes the effect of exchange in the statistical approximation. Rose has reported that the use of a relativistic Hartree calculation made little difference[17]. In the absence of a quantitative estimate of the effect of various potentials, we decided to use a different and hopefully better potential. Fortunately, a complete Hartree calculation for all elements has been reported by Herman and Skillman[30]. They made a non-relativistic self-consistent field calculation including exchange in the Slater "free electron exchange approximation"[31,32]. Slater utilizes the fact that for a free electron gas the exchange potential is only dependent on the local density[33,34],

$$V^{\text{exch}}(r) = -6\left[\frac{3}{8\pi}\rho(r)\right]^{1/3} . \qquad (14)$$

Since the free electron approximation only depends on the density, it cannot cancel the self-interaction of the electron in the outer region of the atom; therefore, Herman and Skillman employed the trick, due to Latter[35], of defining the self-consistent potential equal to α/r beyond the point where it reaches this value. Herman and Skillman have corrected their binding energies for relativistic and spin-orbit perturbations, finding good agreement with x-ray measurements. By using the Dirac Equation, spin-orbit and relativistic effects are

included directly. Since the Herman and Skillman self-consistent potential is associated with the Schrödinger Equation, we expect that our binding energies will be increased. The "non-relativistic" charge distribution is not as contracted as in the actual case, so the shielding is underestimated in heavy atoms. We find, in fact, that the K shell binding energies are too large by 0.5 to 1 keV above Z = 70, the binding energy ranging from 60 to 130 keV. The effect in the L shell is reduced roughly by a factor of five. Liberman and Waber have reported calculations identical to those of Herman and Skillman, except that they use the Dirac Equation instead of the Schrödinger Equation[36]. They were able to get excellent agreement with the x-ray values. While the program we will describe below is the largest part of a self-consistent field calculation, it was felt that the Herman and Skillman potential was adequate as an improvement over the T-F-D potential.

Sliv has reported that while the use of a finite nuclear charge distribution has a drastic effect on the conversion coefficients, a change of the "radius" by 10% results in less than a 2% effect in the conversion coefficient[16]. For ease in finding series solutions at the origin, we used a uniform charge distribution with a radius $R = 1.2A^{1/3}10^{-13}$ cm. The series solution near the origin is of the form

$$g = \left(\frac{r}{R}\right)^{|\kappa|} \sum_{n=0}^{\infty} a_n (r/R)^{2n}$$
$$f = \left(\frac{r}{R}\right)^{|\kappa|} \sum_{n=0}^{\infty} b_n (r/R)^{2n+1} \qquad (15)$$

for $j = \ell + 1/2$ or $\kappa < 0$ solutions, and f and g interchanged for $j = \ell - 1/2$ or $\kappa > 0$ solutions. See Appendix I for notation

concerning the Dirac Equation. Substituting Eq. (15) into the Dirac Equation we find a pair of coupled recurrence relations which are solved numerically for the first 20 coefficients. The step size is roughly 1 Fermi, so 5-7 steps are computed by series inside the nucleus.

The solution, having been started by the power series expansion, was continued by a finite difference scheme . The Adams-Moulton formula was used[37].

$$y_{n+1} = y_n + \frac{\Delta}{24} (9\dot{y}_{n+1} + 19\dot{y}_n - 5\dot{y}_{n-1} + \dot{y}_{n-2}) . \qquad (16)$$

This difference equation is "closed", that is, to calculate y_{n+1} one needs not only y_n, $\dot{y}_n$, $\dot{y}_{n-1}$, $\dot{y}_{n-2}$, but also $\dot{y}_{n+1}$. Usually, a predictor formula is used to get $\dot{y}_{n+1}$, often the Adams-Bashforth formula in this case; and one finds $\dot{y}_{n+1}$ from the differential equation. Then Eq. (16) is iterated for y_{n+1}; in digital computer practice, usually one iteration is performed. For linear differential equations, it is convenient to proceed differently. We first reduce the differential equation (5) to the form:

$$\dot{y}^{(i)} = A(x)_{ij}\, y^{(j)} \qquad (17)$$

or

$$\bar{\dot{y}} = \hat{A}\, \bar{y}, \qquad (18)$$

then Eq. (16) becomes

$$\bar{y}_{n+1} = \bar{y}_n + \frac{\Delta}{24} (9\, \hat{A}_{n+1}\, \bar{y}_{n+1} + 19\, \bar{\dot{y}}_n - 5\, \bar{\dot{y}}_{n-1} + \bar{\dot{y}}_{n-2}) \qquad (19)$$

or

$$\bar{y}_{n+1} = \hat{M}^{-1}\left(\bar{y}_n + \frac{\Delta}{24} (19\ \bar{\dot{y}}_n - 5\ \bar{\dot{y}}_{n-1} + \bar{\dot{y}}_{n-2})\right) \tag{20}$$

where

$$\hat{M} = \left(\hat{I} - \frac{9\Delta}{24}\ \hat{A}_{n+1}\right) . \tag{21}$$

When the order of M is low enough or if M has a simple enough form, Eq. (20) is very attractive. It is equivalent to iterating the Adams-Moulton formula to its limiting solution, and yet requires fewer arithmetic operations than using the Adams-Bashforth and the Adams-Moulton formulae together once.

The radial co-ordinate was scaled as in the Thomas-Fermi Equation,

$$r = \mu x = 1/2 \left(\frac{3\pi}{4}\right)^{2/3} Z^{-1/3}\ x \quad . \tag{22}$$

A mesh size of approximately 1 Fermi was used to start. The mesh size was doubled every 100 steps for a total of 5 blocks. This mesh scheme is nearly logarithmic and is suitable for atomic wave functions. After five blocks the step size was fixed since it was also desired to compute the free electron wave function (with energies up to 2 MeV), at the same mesh points.

The inward solution was started by deriving the ratio of f to g from the differential equation. Enough points to use the difference scheme were found by the Runge-Kutta method. The differential equation was integrated inward until the match point was reached where approximately $E - V(r) > 0$. The solution on the right was then

normalized so the large components were equal. From the mismatch of the small component, a correction to the eigenvalue was predicted. If W is the trial energy and ΔW the error, then

$$\frac{f^L}{g^L} \equiv \rho_L(W + \Delta W) = \rho_R\ (W + \Delta W) \equiv \frac{f^R}{g^R}\ . \tag{23}$$

Rose has shown that[38]

$$\frac{\partial \rho^L}{\partial W} = -\frac{1}{g_L^{\,2}} \int_0^r (g^2 + f^2)\ dr \tag{24}$$

and

$$\frac{\partial \rho^R}{\partial W} = -\frac{1}{g_R^{\,2}} \int_n^\infty (g^2 + f^2)\ dr. \tag{25}$$

Expanding Eq. (23)

$$\Delta W = \frac{\rho_L - \rho_R}{\frac{\partial \rho^R}{\partial W} - \frac{\partial \rho^L}{\partial W}}\ . \tag{26}$$

Now, using Eqs. (24) and (25)

$$\Delta W = \frac{g(f^L - f^R)}{\int_0^\infty (f^2 + g^2)dr}\ . \tag{27}$$

The integration of the Dirac Equation was iterated until the predicted ΔW was less than $10^{-8}\ m_e$.

The calculation of the continuum wave function was similar, except that the differential equation was always integrated outward. Normalization was effected by comparing the calculated solution with WKB solutions of the Dirac Equation[39].

$$g = N\,A(r)\,\sin\,(K(r)\,r + \delta)$$

$$f = N\,B(r)\,\cos\,(K(r)\,r + \delta) \qquad (28)$$

A(r) and B(r) are the WKB amplitudes. The procedure then is to find as a function of r,

$$N^2 = \frac{g^2}{A(r)^2} + \frac{f^2}{B(r)^2} \; . \qquad (29)$$

The quantity N^2 is a constant plus a small ($< 10^{-3}$) oscillating component. N^2 was averaged over one electron wavelength to give the square of the normalization. The spherical Bessel functions were calculated from power series expansions in the region near the origin where the "centrifugal" term $\ell(\ell + 1)/r^2$ is large. Outside this region their definitions in terms of sines and cosines were used, e.g.,

$$f_1(Z) = \frac{\sin\,(Z)}{Z^2} - \frac{\cos\,Z}{Z} \; . \qquad (30)$$

To increase the speed of computation, the recurrence relations for the circular functions were used;

$$\sin(X + \Delta) = \sin X \cos(\Delta) + \cos X \sin(\Delta) \; . \qquad (31)$$

In this manner the sines and cosines need be calculated only once. Having now computed the wavefunctions and the Bessel functions, the radial integrals were done using Simpson's Rule. The program was designed to compute conversion coefficients for M1, M2, E1, and E2 multipoles, although the extension to other multipoles is trivial.

C. Comparison with Previous Calculations

Our calculations show that in general the agreement with Sliv's result is significantly better than with Rose's. A general statement is that our results agree with Sliv's to within 5%, while we often differ more than 10 to 20% with Rose's values. Specifically, for comparison, calculations were made for M1 and E2 radiation in the L shell as a function of transition energy and atomic number. The ratios SLIV/CIT,(S), and ROSE/CIT,(R), are shown in Fig. 1. The good agreement with Sliv should be noted, as well as the systematic bias toward larger values than Sliv. Since we did not include any estimate of penetration as Sliv did, it is necessary to investigate this last point. In two cases the surface current estimate was used to determine its contribution to the discrepancy between Sliv's and our results. For M1 conversion at 0.2 m_e energy in the L1 shell as a function of atomic number, the addition of the surface current term reduced the discrepancy to less than 1% for $Z < 90$. For M1 conversion in the L2 shell with Z fixed the discrepancy is reduced at low energies. At energies above 500 keV the disagreement is increased. The oscillation of the integrand makes the computation of internal conversion coefficients at high energies difficult. Sliv has already indicated that their calculations are of reduced accuracy at high energies[16].

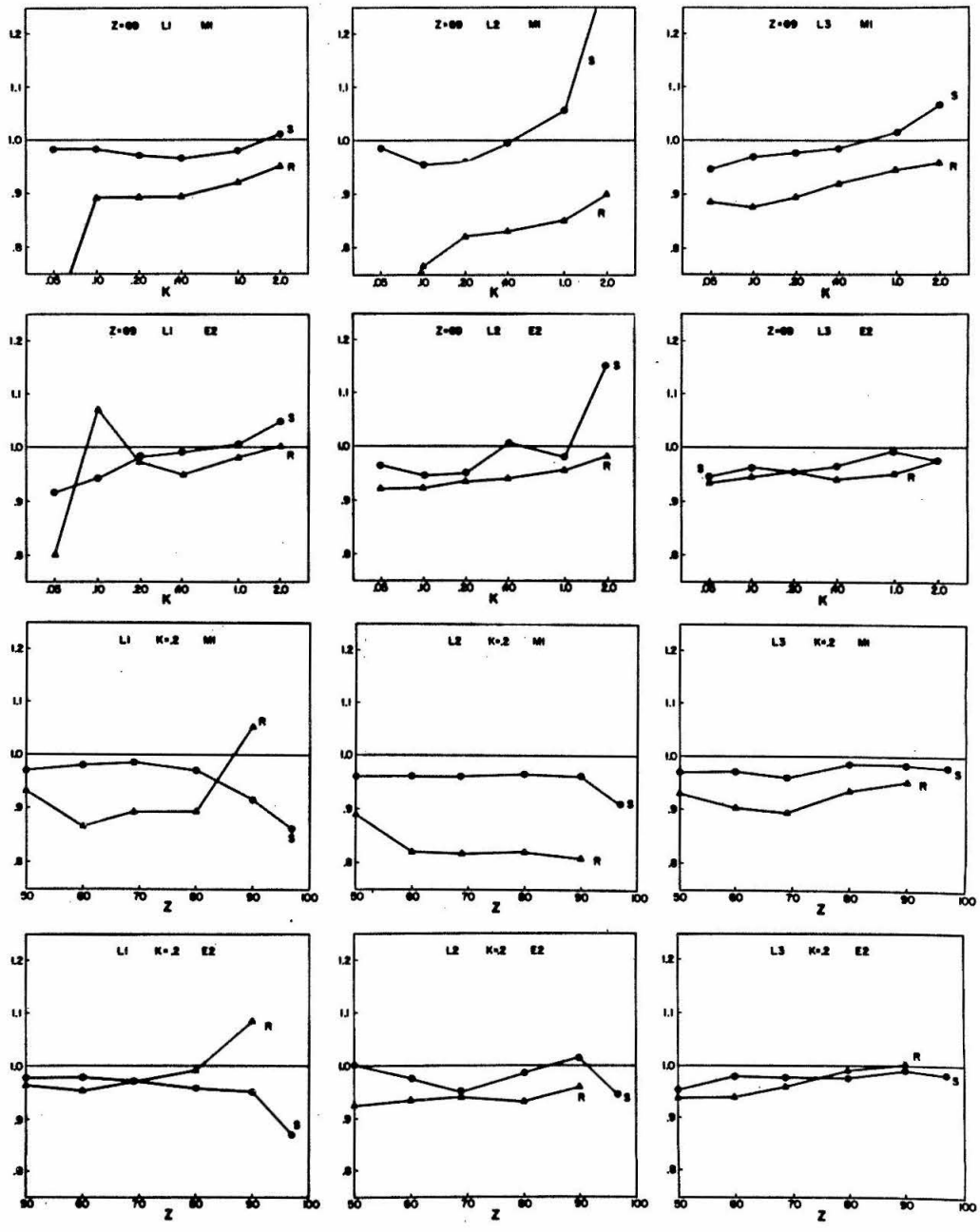
Z=00 L1 M1
Z=00 L2 M1
Z=00 L3 M1
Z=00 L1 E2
Z=00 L2 E2
Z=00 L3 E2
L1 K=.2 M1
L2 K=.2 M1
L3 K=.2 M1
L1 K=.2 E2
L2 K=.2 E2
L3 K=.2 E2
S
R
K
Z

Fig. 1

III. GENERAL ASPECTS OF INTERNAL CONVERSION INVOLVING PENETRATION EFFECTS

A. Form of the Operators

As was shown in Chapter II and Appendix II, the nuclear matrix elements that occur for electrons penetrating the nucleus are of the form,

$$M_L^m\ (M) = \int \vec{j}_n \cdot \vec{L}\ Y_L^m\ r^n \tag{32}$$

for the magnetic case, and

$$M_L^m\ (\vec{j}\cdot\vec{\nabla}) = \int \vec{j}_n \cdot \vec{\nabla}\ Y_L^m\ r^n \tag{33}$$

$$M_L^m\ (\vec{j}\cdot\vec{r}) = \int \vec{j}_n \cdot \vec{r}\ Y_L^m\ r^n \tag{34}$$

for the electric case. As is well known, introducing the nuclear current

$$\vec{j}_n = -\frac{e}{2iM_p}\left((\nabla\ \psi_f^*)\psi_i - \psi_f^*\nabla\psi_i\right) + \mu\vec{\nabla}\ x\ (\psi_f^*\ \vec{\sigma}\ \psi_i) \tag{35}$$

one finds for the gamma-ray magnetic transition operators[23]

$$\frac{e}{2M}\left(g_s\vec{\sigma} + \frac{2}{L+1}\ g_L\ \vec{\ell}\right) \cdot \vec{\nabla}\ (r^L\ Y_L^m). \tag{36}$$

Also, the continuity equation,

$$\vec{\nabla}\cdot\vec{j} + i\ k\ \rho = 0 \tag{37}$$

can be used to derive a very general reduction of electric transition operators for gamma-ray emission[23],

$$M_L^m\ (e) = \int \rho\ Y_L^m\ r^L\ dV\ . \tag{38}$$

The electric and magnetic penetration operators are reduced in a similar way to forms that are more easily interpreted than Eqs. (32) - (34). In Table 1 we give the various operators and their origins. A short resume of the nuclear model used is given before we discuss the various entries in Table 1.

B. Nuclear Model

The nuclei that are discussed in this thesis are best described in terms of the rotational model. This successful model has been adequately reviewed[45-47].

The theory may be outlined as follows: some nuclear states may be described as collectively deformed, possessing collective and intrinsic co-ordinates. The collective co-ordinates describe rotation and vibration. The intrinsic co-ordinates describe single-particle motion. This single-particle motion has been successfully represented by a "deformed" shell model Hamiltonian:

$$H = \frac{p^2}{2M} + M\omega_0^2(x^2 + y^2 + z^2) + \epsilon m\omega_0^2 z^2 + C\,\vec{\ell}\cdot\vec{s} + D\,\vec{\ell}\cdot\vec{\ell}. \quad (39)$$

Residual short range interactions are introduced by using a pairing force and the B.C.S. formalism. The model wavefunction is written as

$$\psi^M_{IK} \sim D^M_{IK}\,\chi_K + (-1)^{I-K} D^m_{I-K}\,\chi_{-K}\,. \quad (40)$$

Eigenfunctions of the intrinsic Hamiltonian, Eq. (39) are conveniently expanded in a basis set of eigenfunctions of the axially symmetric harmonic oscillator[48]. For actual nuclei, the deformation is sufficiently large that one component of the eigenfunction is

		γ-Ray	Penetration
E1	$j\cdot\nabla$	$\bar{r}$	$r^2\bar{r}$
	$j\cdot r$		
	conv.	$O(kr) \times j\cdot\nabla$	$r(\bar{r}\cdot\bar{p} - 2i)$
	spin	$O(kr) \times j\cdot\nabla$	$\bar{r} \times \bar{\sigma}$
	$l\cdot l$	—	—
	$l\cdot s$	—	—
E2	$j\cdot\nabla$	$r^2 Y_2^m$	$r^4 Y_2^m$
	$j\cdot r$		
	conv.	$O(kr) \times j\cdot\nabla$	$r^2 Y_2^m(\bar{r}\cdot\bar{p} - 5i)$
	spin	$O(kr) \times j\cdot\nabla$	$\bar{\sigma}\cdot(\bar{L} r^2 Y_2^m)$
	$l\cdot l$	—	—
	$l\cdot s$	—	—
M1	conv.	$\bar{L}$	$r^2\bar{L}$
	spin	$\bar{\sigma}$	$2r^2\bar{\sigma} - (\bar{\sigma}\cdot\bar{r})\bar{r}$
	$l\cdot l$	$r^2\bar{L}$	$r^4\bar{L}$
	$l\cdot s$	$(\bar{\sigma}\cdot\bar{r})\bar{r} - r^2\bar{\sigma}$	$((\bar{\sigma}\cdot\bar{r})\bar{r} - r^2\bar{\sigma})\, r^2$

conv: $j = e/2m\,(f^*\bar{p}\,i + (\bar{p}f)^*i)$

spin: $j = \mu\,\bar{\nabla} \times (f^*\bar{\sigma}\,i)$

l·l : current of $\bar{L}^2$ term in Hamiltonian

l·s " " $\bar{L}\cdot\bar{S}$ " " "

Table 1

dominant. Its quantum numbers may be used to characterize the entire wavefunction; they are called the "asymptotic quantum numbers". For example, a state will be labeled $[N\ N_z \Lambda]\Sigma$. N denotes the total number of oscillator quanta; N_z , that number of quanta corresponding to the z-co-ordinate degree of freedom; and Λ, the eigenvalue of L_z. Σ labels the spin state. The projection of the intrinsic angular momentum upon the intrinsic z-axis is the "K" quantum number:

$$K = \Lambda + \Sigma \ . \tag{42}$$

There are two major classifications of selection rules. The first and most fundamental to the collective model is the "K-selection rule". If a transition is between two bands whose K quantum numbers differ by an integer exceeding the tensor rank of the transition operator, then the transition is strictly forbidden. The excess is called the "degree" of K-forbiddenness. Terms, such as the Coriolis force, which are neglected in first approximation induce K impurities in the levels. Each degree of K-forbiddenness is said to hinder a transition by roughly a factor of 100. The existence of nearby bands may reduce this estimate in any particular case. The K selection rule has the character that if a transition is K forbidden then the penetration contributions will be forbidden also. Of course, it may happen that the gamma-ray transition amplitude involving the K impurities is still hindered to a greater extent than the penetration amplitude.

The other cause of retardation is the "asymptotic selection rule". The asymptotic selection rule is one which forbids a transition

between the dominant parts of the wavefunction. In the usual shell model there are also rules leading to single particle hindrances. The L-forbiddenness rule is the easiest to appreciate, but, in general, they are not readily noticed. The situation in the case of the deformed shell model is different; the asymmetric oscillator quantum numbers give an immediate indication of the hindrance. Asymptotic selection rules usually imply a hindrance of 25-100. The penetration operators in Table 1 are often allowed in several important cases. An electric transition between states involving spin flip is asymptotically hindered:

$$[N\ N_z \Lambda] + \rightarrow [N' N'_z \Lambda'] - . \qquad (43)$$

The penetration operators which arise from the spin current, it is noticed (Table 1), do not have this limitation. In general, the more complex construction of the penetration operators results in a broader range of allowed transitions. The $(\vec{\sigma}\cdot\vec{r})\ \vec{r}$ M1 penetration operator should be effective in those transitions which are L-forbidden.

C. Characteristics of Electric Transitions

The general dominance[49,50] of the $\vec{j}\cdot\vec{r}$ type of penetration contribution over the $j\cdot\nabla$ type in electric transitions results from three causes[51,52]. Superficially, the situation looks the reverse and has been the source of some confusion[50]. The weighting of the $j\cdot\nabla$ penetration amplitude is formally $0(KR)$ larger than the $j\cdot r$ amplitude. This prompted Nilsson and Rasmussen to neglect the $\vec{j}\cdot\vec{r}$ type term.[50]. The major part of the $j\cdot\nabla$ weighting has a factor $ff' + gg'$. (See

Appendix II.) For the $L_I(2S_{1/2})$ and $L_{II}(2P_{1/2})$ shells a curious thing happens. Since in these shells, the electron penetrates the nucleus to a greater extent than in the L_{III} shell $(2P_{3/2})$, one expects these shells to show the largest penetration effects. But for these shells the most important partial waves from the point of view of amplitude at the nucleus are the $P_{1/2}(\kappa = 1)$ and $S_{1/2}(\kappa = -1)$. (Appendix I) From the recurrence relation for the power series solution of the Dirac Equation, we find

$$\rho(\kappa = -1) = \frac{f_{-1}}{g_{-1}} = -\frac{R_0(W - 1) + \frac{3\alpha z}{z}}{3} \tag{44}$$

and

$$\rho(\kappa = +1) = \frac{f_{+1}}{g_{+1}} = \frac{3}{R_0(W + 1) + \frac{3\alpha z}{z}} \tag{45}$$

or

$$\frac{1}{\rho(\kappa = +1)} = -\rho(\kappa = -1) + \frac{2R_0}{3} \quad , \tag{46}$$

Therefore, for the predominant partial wave,

$$\begin{aligned} f_1 f_{-1} + g_1 g_{-1} &= f_1 g_{-1}\left(\frac{f_{-1}}{g_{-1}} + \frac{g_1}{f_1}\right) \\ &= f_1 g_{-1}\left(\rho_{-1} + \frac{1}{\rho_1}\right) \\ &= f_1 g_{-1}\left(\frac{2R_0}{3}\right) \\ &\approx -\frac{1}{22} f_1 f_{-1} \cdot \end{aligned} \tag{47}$$

The $j\cdot\nabla$ weighting coefficient therefore is reduced usually by

approximately 22. Thus, the contribution from the $j\cdot\nabla$ term in the other partial waves is comparable to these transitions, ($S_{1/2} \rightarrow P_{1/2}$) and ($P_{1/2} \rightarrow S_{1/2}$). Furthermore, the L_{III} shell should have comparable admixtures of penetration terms. This is contrary to the experimental evidence[53].

Reconsideration of the $j\cdot r$ terms provided the answer to this problem[18,51,52]. The estimation of the nuclear matrix elements shows that the $j\cdot r$ type is larger than the $j\cdot\nabla$ type by a factor ω/k, where ω is a characteristic shell model energy (i.e., oscillator constant) and k is the transition energy. Assuming reasonable values for ω and k,

$$\omega \sim 8 \text{ MeV}$$

$$k \sim 100 \text{ keV}$$

we see that $\omega/k \sim 80$ is a significant factor. Also, the spin flip property of the $j\cdot r$ operators (Table 1) is in many cases decisive. There is one further reason that $j\cdot r$ matrix elements are expected to be larger than the $j\cdot\nabla$ type. The effect of pairing correlations on the transition rates is to modify the single-particle amplitude by a factor $(U_i U_f \pm V_i V_f)$:[53]

$$M_{fi}^{\text{pair}} = M_{fi}^{\text{single particle}} \times (U_i U_f \pm V_f V_i). \qquad (48)$$

The U's and V's are the pair occupation amplitudes[46]. The + sign refers to operators that reverse sign under time-reversal (e.g., $\vec{\sigma}$). The - sign is used for operators invariant under time-reversal (e.g., $\vec{r}$). Therefore, one may expect electric gamma-ray transitions to be

hindered; while the magnetic gamma-ray transitions are not affected to any great extent. The $j\cdot\nabla$ type penetration operator gives rise to a matrix element that is invariant under time-reversal just as in gamma-ray emission. The $j\cdot r$ type, however, can be shown to change sign under time-reversal. Therefore, in the usual experimental cases where one studies retarded E1 transitions, the $j\cdot r$ penetration term is not hindered by the pairing factor as is the $j\cdot\nabla$ type. Hindrances as large as 100-1000 may occur. Collective E2 transitions do not have this pairing factor.

We may summarize then, the reasons for the dominance of the $\vec{j}\cdot\vec{r}$ terms as (1) cancellation of the $\vec{j}\cdot\vec{\nabla}$ weighting coefficient, (2) the $\vec{j}\cdot\vec{r}$ matrix elements are intrinsically larger than the $\vec{j}\cdot\vec{\nabla}$ type, and, (3) the time-reversal property of the $\vec{j}\cdot\vec{r}$ matrix element does not lead to retardations due to pairing correlations. Having shown that the $j\cdot r$ type term is expected to be dominant, we can now explain the observed pattern of E1 penetration effects in the L shell. The electron weighting factor for the $j\cdot r$ type penetration amplitude is $(f\,g' - g\,f')$. (Appendix II) This factor does not have any cancellation properties as did the $(f\,f' + g\,g')$ factor for the $j\cdot\nabla$ terms. The lower angular momentum states for the free electron that occur in L_I and L_{II} shell conversion can now dominate. All these points concerning penetration effects in E1 conversion have been elegantly demonstrated in experiments in this laboratory performed by R. Hager[54].

IV. EXPERIMENTAL TECHNIQUE

A. Magnetic Spectrometer

Two instruments were used to perform the experiments we will describe here. The bulk of the work was performed on the new Caltech $\pi\sqrt{2}$ spectrometer. The other instrument was a Lithium drifted Ge semiconductor detector , the properties of which have been extensively reported in the literature[40]. The efficiency of this device for gamma rays has been carefully calibrated in this laboratory[41].

The most significant property of the Caltech $\pi\sqrt{2}$ spectrometer is that it is iron free. The absence of an iron yoke, while greatly increasing the power requirements, allows one to form the magnetic field with much greater precision. The Caltech $\pi\sqrt{2}$ spectrometer is a scaled-down version of a larger machine at Chalk River, Ontario[42,43]. Figures 2 and 3 show details of the spectrometer. The highest momentum resolution attained was 0.02% for $\Delta P/P$. This was with the 113.0 keV L3 line in Hf^{177}. The equivalent energy width is 40 eV. Figure 4 shows this line. The instability of the power supply and energy degradation in the source are the principal cause of spurious broadening of the line image. Careful control of the thermal and mechanical instabilities in the reference voltage and associated resistors, allows one to reach a DC current stability of $1:10^5$. At .02% momentum resolution, this represents 1/20 of the line width. The instabilities tend to be of a long-term nature; therefore, in comparing the intensities of two lines at this resolution, errors as

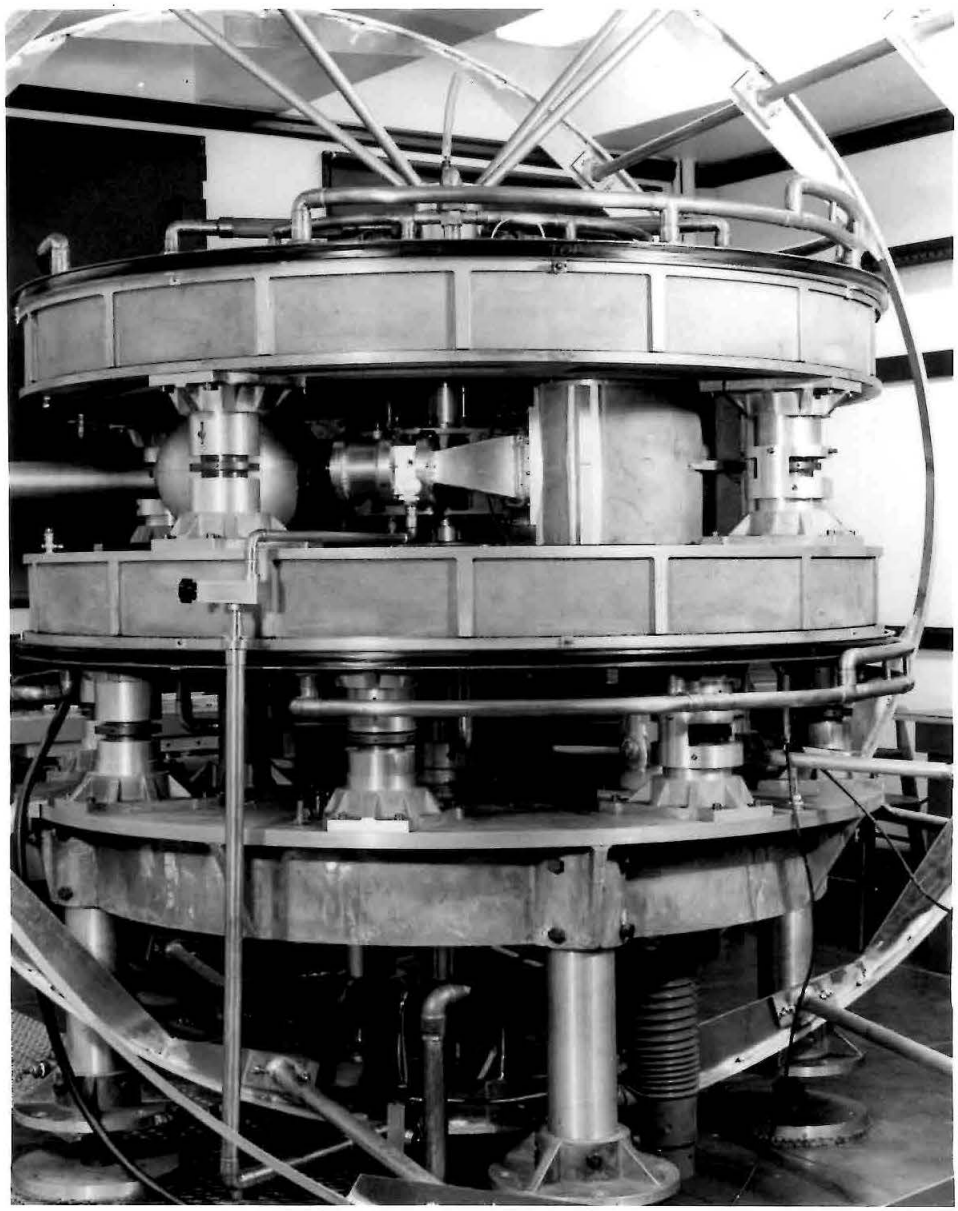

Fig. 2

$\pi\sqrt{2}$ Magnetic Spectrometer

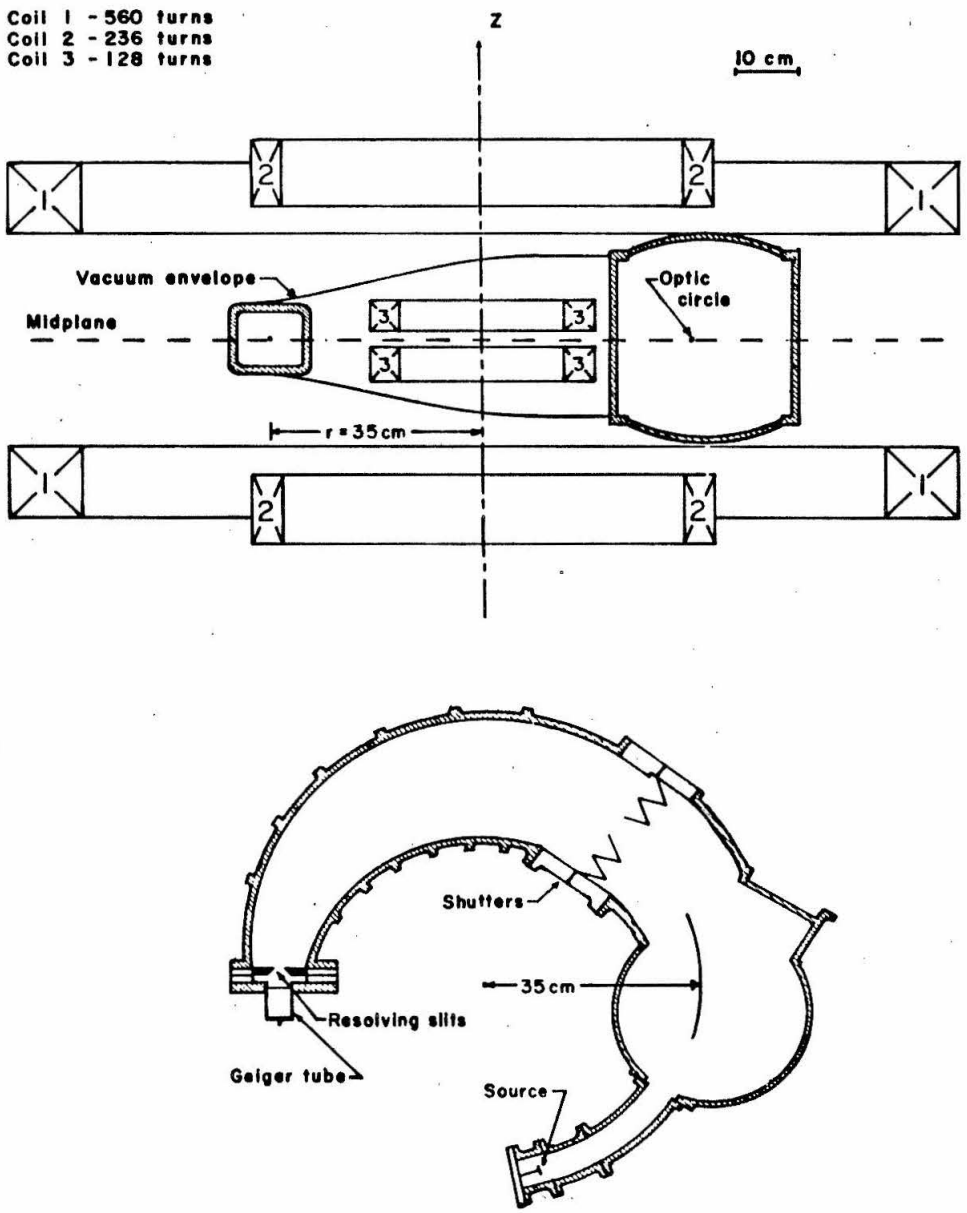

Fig. 3

Views of Spectrometer Coils and Vacuum Chamber

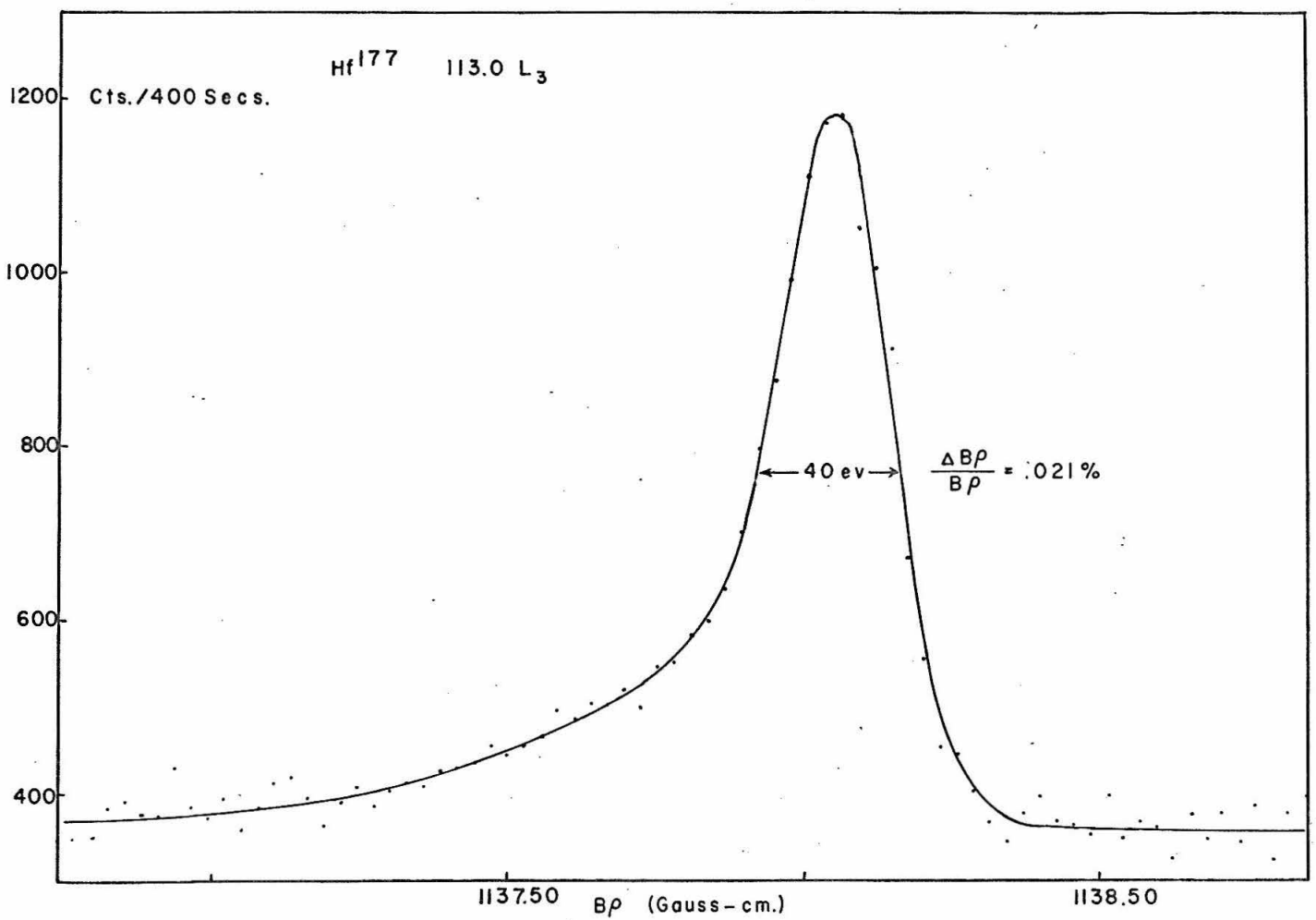

Fig. 4

Hf^{177} 113.0 keV L_3 Internal Conversion Spectrum

large as 5% may arise. This is overcome by the method of data collection to be described.

B. Detectors

The electron detector should also have good stability as well as high efficiency. Detectors that have been used are Geiger tubes, Anthracene scintillators, and drifted Si detectors. An Anthracene scintillator is capable of high counting rates and has fairly constant efficiency. The strong magnetic field present necessitates a long light pipe, thereby requiring the electron energy to be greater than 60 keV. For the work to be reported here, the counting rates were low enough that a Geiger tube could be used. The stability of a Geiger tube is measured by the fractional change in counting rate per 100 volt change in operating voltage. The counting rate versus operating voltage characteristic exhibits a "plateau". Our requirements of a thin window and large aperture could not be satisfied by commercially available counters. After considerable effort the following "formula" was found. The body of the counter was a brass tube 4" long with 2" inside diameter. The tube was cleaned and then oxidized with dilute nitric acid. The electrons entered an end window. The endplates were constructed of Lucite to reduce end- effects. The anode was 3 mil stainless steel wire. Mathieson 1.3% Butane, 98.7% Helium gas, was flowed continuously through the counter. Windows were made of Mylar (500 $\mu gms/cm^2$) and Formvar (25-100 $\mu gms/cm^2$). The gas pressure varied from 10 cm to 80 cm. Hg. Plateau slopes of 0.2 - 0.5%/100 volts were obtained. The counter would operate continuously for several months.

In order to decrease the counting rate due to background radioactivity, the following system was sometimes used. If insulating beads are placed along the wire in intervals (five to six), the ionization occuring during a Geiger pulse can be localized. Only an electron traveling the length of the tube will fire all sections. Since background radiation most probably fires only one or two sections, it is possible with a pulse-height analyzer to discriminate against background radiation. A reduction of the background by a factor of ten was possible while still counting 90% of the electrons from the spectrometer traveling lengthwise down the Geiger tube.

C. Source Preparation

The other cause of line broadening is due to source thickness, which can only be reduced by using sources of very high specific activity, deposited in a thin homogeneous layer. Preparing β sources is the most difficult part of β spectrometry. Enriched isotopes and high flux reactors are essential in obtaining high specific activities. 100% Ta^{181}, > 90% Hf^{180}, and 30 - 35% Yb^{168} were used to make 115 day Ta^{182}, 45 day Hf^{181}, and 32 day Yb^{169}. The 5 day Ta^{183} activity, made by double neutron capture, was allowed to decay. Of course, the capture cross-section and half-life determine the specific activity in each instance. When one has enough material, the best technique for making β sources is by evaporation[44]. We found that the fluorides of the above isotopes, having a high boiling point and little tendency to form hydrates, made the most easily controlled and stable evaporations. Platinum evaporation boats were required. These were

approximately 1.5 cm long, .5 cm deep, and 1 mm wide. The evaporation was performed at 10^{-5} mm. pressure. Evaporation usually occurred at approximately 1000 - 2000°C. The evaporated material was collected on an aluminum foil 2 to 5 mm above the boat. The duration of the evaporation and height of foil can be used as variables in determining source thickness. The energy of the electron line and the resolution which is desired are important considerations. Once the required length and width of the source are calculated, it is cut with scissors and mounted on a 0.025 inch thick aluminum plate. While the thickness of the backing is an important problem if one is measuring the electron spectrum in β decay, it is not important for the study of monoenergetic internal conversion lines.

D. Data Collection

The errors in the relative intensities of two lines due to instability of the detector system or in the current supply were eliminated by the technique of stepping continuously over the region being scanned. A similar method for data collection in Mössbauer spectroscopy had previously been developed by E. Kankeleit[72]. If there are many sweep cycles, then drifts contribute only to the line width, but errors in the relative intensities are averaged to zero. We feel this system is essential for obtaining relative electron intensities, accurate to 1%. Scanning of weak lines in the presence of a large background is very difficult with short lived isotopes. With this stepping method half-life corrections are virtually eliminated.

V. EXPERIMENTS

A. Results for Magnetic Dipole Cases

In this thesis, we are concerned with penetration effects in M1 transitions in Ta^{181} and Lu^{175}, and anomalous effects in E2 transitions in W^{182}, Ta^{181} and Tm^{169}. The anomalous M1 482 KeV transition in Ta^{181} has been a classic example of M1 penetration effects[55]. This M1 transition is unusually retarded, $\sim 10^6$. The experimental work has been difficult to interpret in terms of penetration effects[55,56], but the recent discovery of theoretical errors in the internal conversion particle parameters require that the $(\gamma\text{-}e_K)$ angular correlation experiments be reinterpreted[57,58]. The observance of parity non-conserving forces in the nuclear potential by use of just this transition[59] has generated further interest in determining the penetration matrix element. The sign of the penetration matrix element is useful in predicting the sign of the parity effect. This will be explained below. In Lu^{175} we have a transition (343 KeV) which is between nuclear states that have the same quantum numbers as those involved in the 482 KeV transition in Ta^{181}. The M1 rate does not appear to be as retarded as for the 482 KeV transition. The determination of the penetration matrix element may be useful in understanding the behavior of these retarded M1 transitions.

Figure 5 shows the level scheme of Ta^{181}. There have been conflicting reports of additional transitions, levels, and alternate placing of transitions. Previous work by the author and others in this laboratory, have confirmed the correctness of Fig. 5[60].

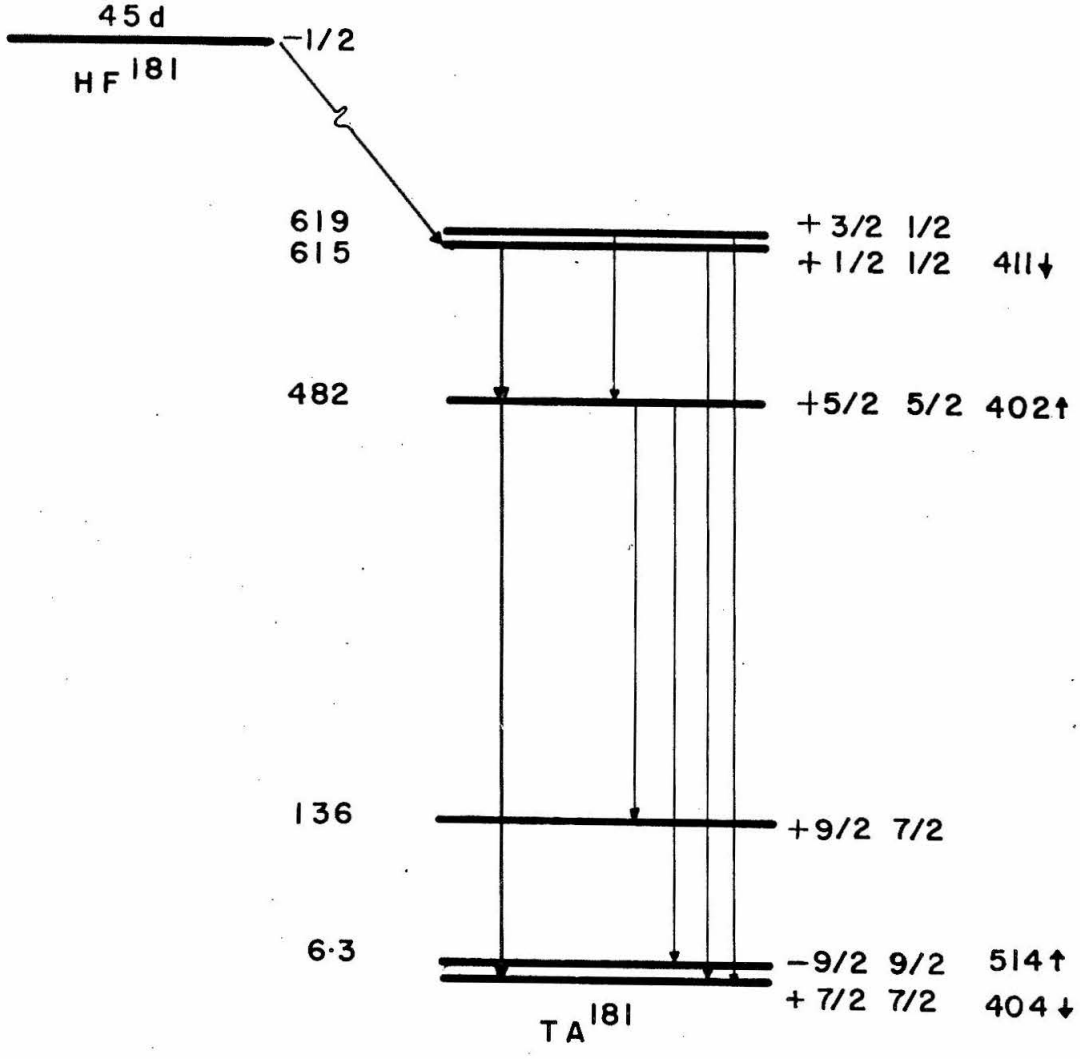

Fig. 5

Level Scheme of Ta^{181}

The 482 KeV transition is seen to go between the $[402]\uparrow$ state and the $[404]\downarrow$ level. The M1 operator is asymptotically hindered:

$$M1 \backsim g_\ell \vec{\ell} + g_s \vec{S} .$$

The simplest operator which is allowed is $\sigma_- x_+ x_-$. The M3 operator $\vec{\sigma}\cdot\vec{\nabla}\,(r^3 Y_3^m)$ or $[\sigma^{(1)} \times r^2 Y_2^m]^{(3)}$, is allowed but is expected to be 10^5 times slower than the observed gamma-ray emission rate. The $(\vec{\sigma}\cdot\vec{r})\vec{r}$ penetration term in internal conversion is allowed. The M1 rate is retarded by approximately a factor of 10^6 with respect to the Weisskopf estimate. This fact, plus the allowed character of the M1 penetration operator makes the 482 KeV transition a good candidate for observing penetration effects. However, since the M1 rate is hindered much more than asymptotic selection rules usually imply, one might expect the penetration amplitude to deviate from nuclear model predictions.

In Figs. 6 and 7 we show the 482 KeV L sub-shell spectrum. In addition, the K/L ratio was measured. The absolute K conversion coefficient was measured by the comparison method described in the experimental section. The results of the experiments on Ta^{181} are summarized in Table 2. Using our conversion coefficient calculations, the conversion data have been analyzed to determine the $\lambda = (M_{pen}/M_\gamma)$. See Fig. 8. The E2/M1 mixing (the vertical lines in Fig. 8) was taken from the work of Grabowski, et al.[56]. The positive and negative solution of λ are equally acceptable with the $\lambda > 0$ solution showing slightly less spread. Fortunately, the (133)γ - (482)K gamma-electron

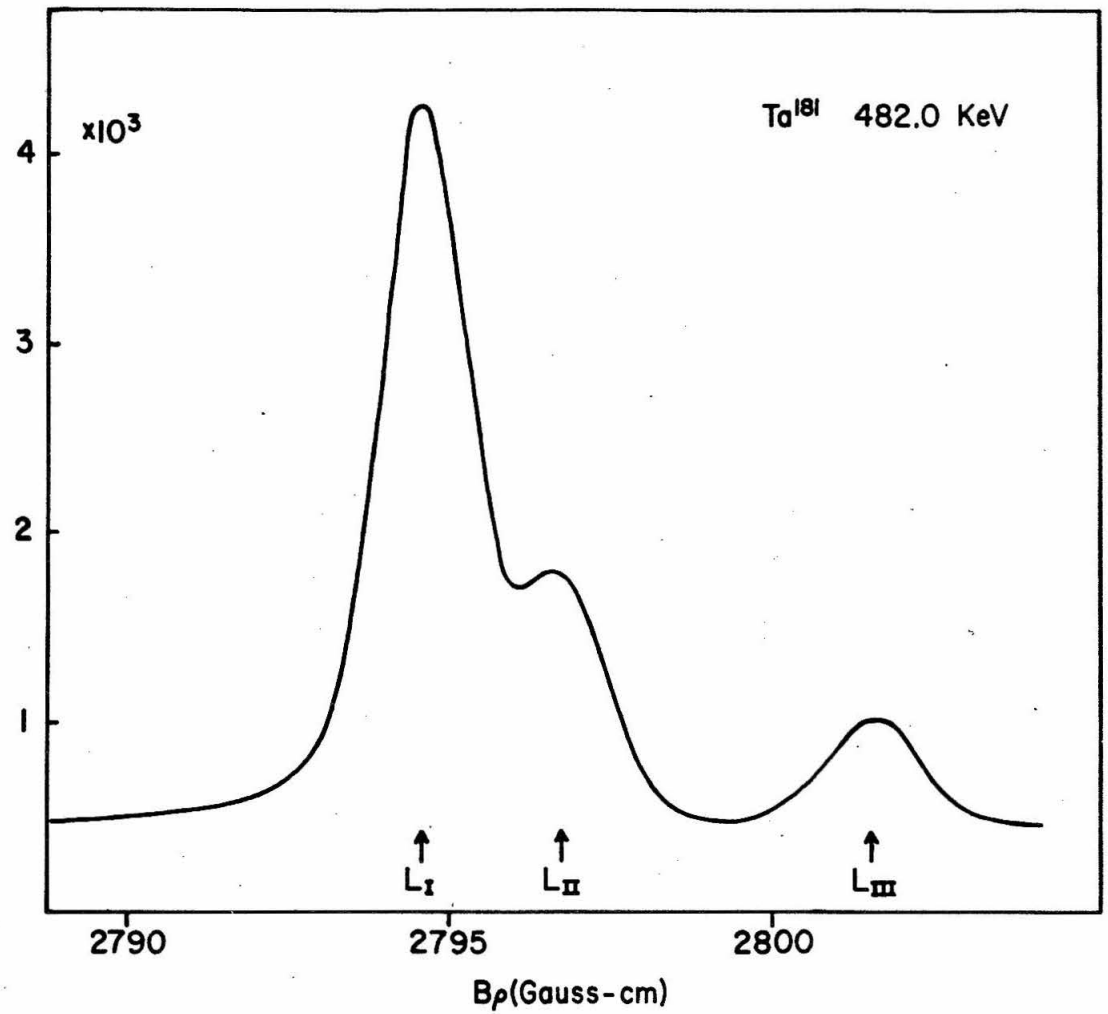

Fig. 6

L-Shell Internal Conversion Spectrum of the 482 keV Line

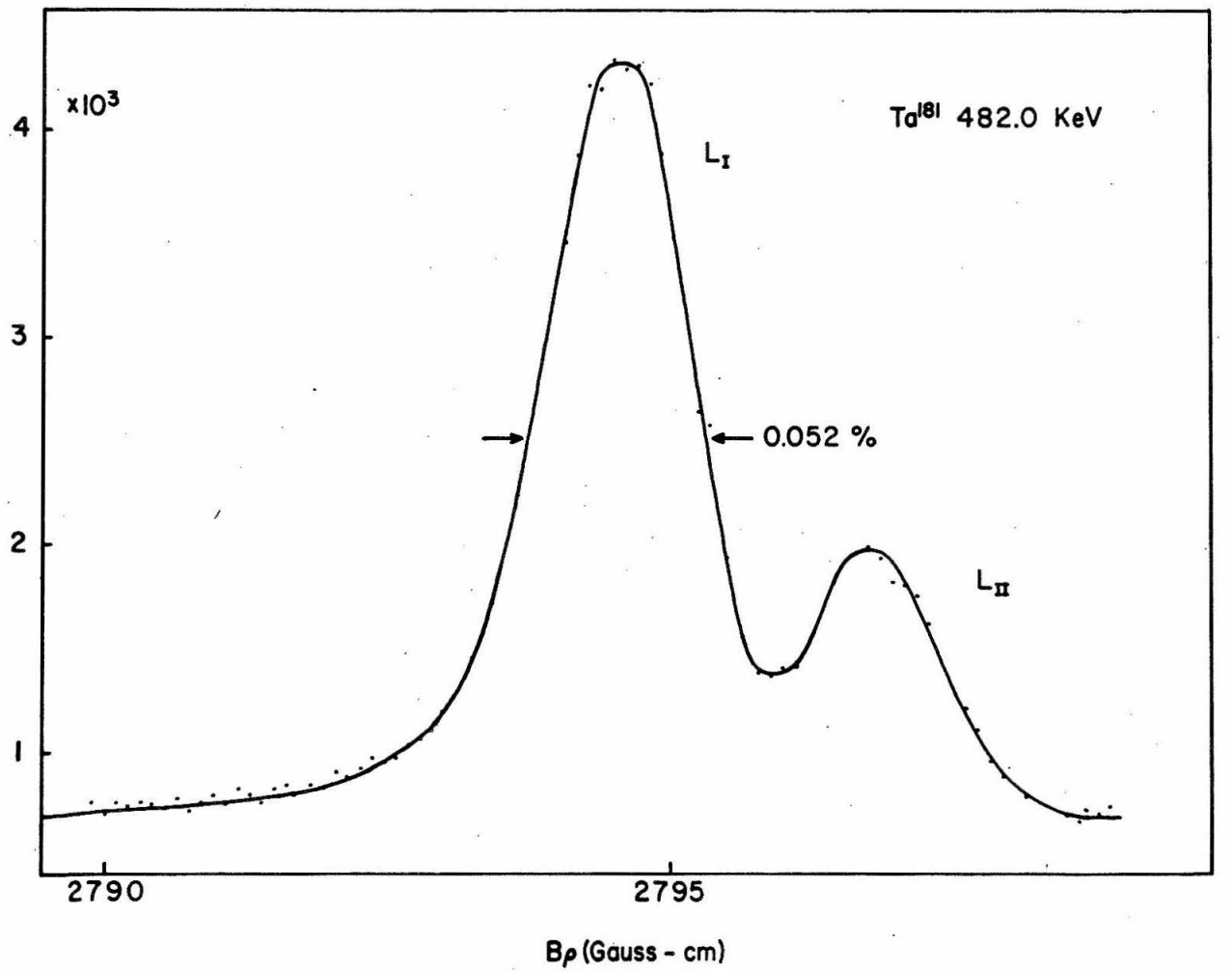

Fig. 7

L-Shell Internal Conversion Spectrum of 482 keV Line

Hf^{181}		482 KeV
L_1/L_2	=	2.92 ± .01
L_1/L_3	=	6.26 ± .3
K / L	=	4.21 ± .2
K	=	0.0239 ± .001

Lu^{175}		343 KeV
L_1/L_2	=	11.0 ± .2
L_1/L_3	=	52.0 ± 2.0
K/L_3	=	345 ± 17
K	=	.098 ± .005

Table 2

Experimental Results for Ta^{181} and Lu^{175}

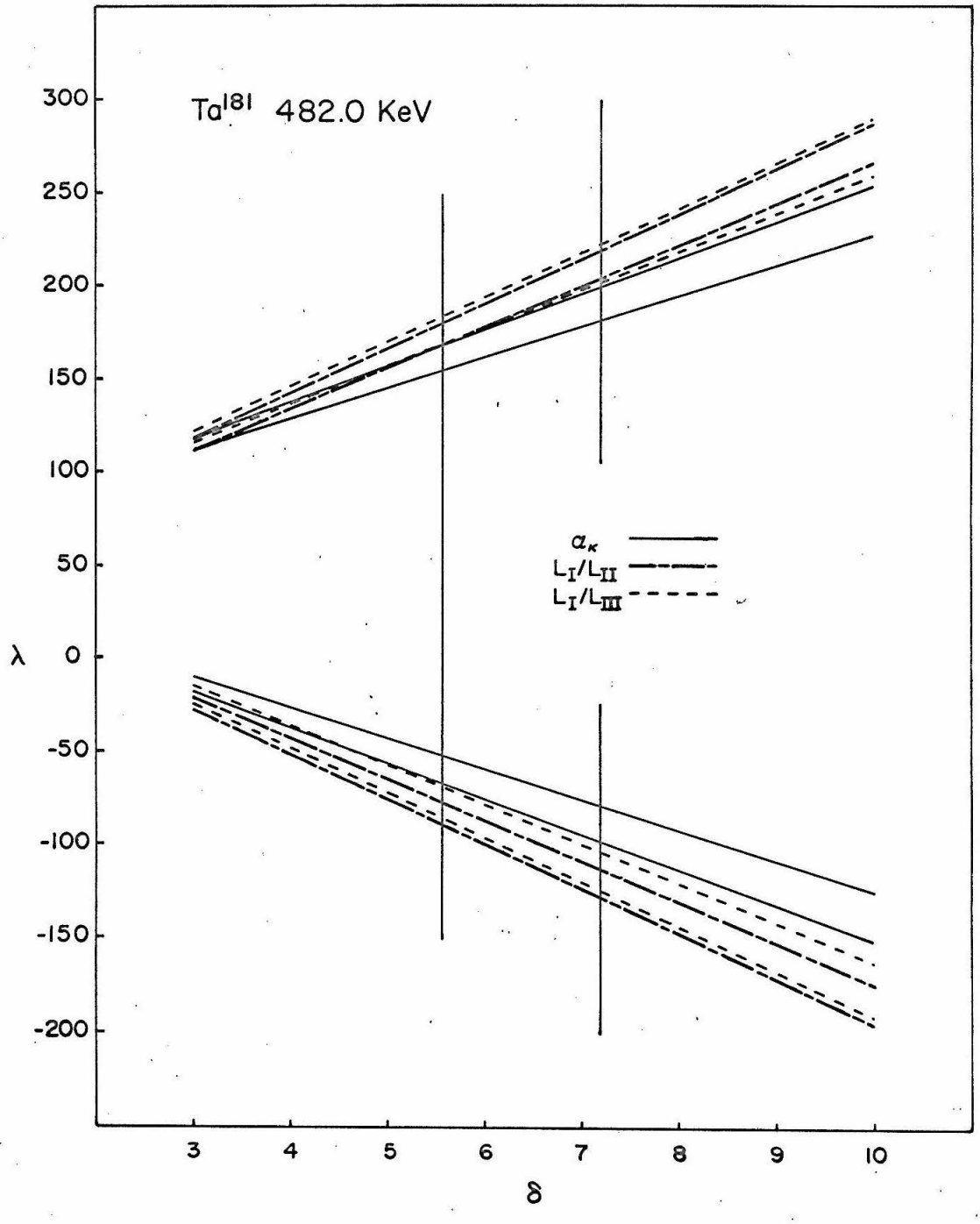

Fig. 8

Variation of λ with E2/M1 Mixing, δ
Lines represent limits due to experimental errors

correlation has been re-analyzed[61] and definitely favors the $\lambda > 0$ solution. The $(\gamma - e_K)$ measurement gives $\lambda = + 210 \pm 30$ in good agreement with our λ:

$$\lambda = + 175 \pm 25 \ .$$

The 343 KeV transition in Lu^{175} is analogous to the 482 KeV transition in Ta^{181}. See Fig. 9. The same measurements that were made in Ta^{181} were repeated in Lu^{175}. See Table 2 and Figs. 10 and 11. The M1 rate is retarded only by a factor of 1000 in this case. A smaller λ is therefore expected. In Fig. 12 we show the variation of λ vs percent E2 for the different data. There may be an effect as large as $\lambda = - 8 \pm 5$. If we assume that the penetration matrix element has the same value in both Ta^{181} and Lu^{175}, which is reasonable, since it is allowed, then we may scale the gamma-ray matrix elements by the lifetimes and energies in order to find a relation between $\lambda(482)$ and $\lambda(343)$.

$$\left| \frac{M_\gamma(343)}{M_\gamma(482)} \right| = \left[\left(\frac{482}{343} \right)^3 \ \frac{1 + \delta^2(482)}{1 + \delta^2(343)} \ \frac{\tau(482)}{\tau(343)} \right]^{1/2}$$

$$= 50$$

	Reference
$\tau(482) = 11 \times 10^{-9}$ s	(62)
$\delta(482) = 6.4 \pm .8$	(56)
$\lvert\delta(343)\rvert = .3$	Taken from Fig. 12

$$|\lambda(343)| = |\lambda(482)| \left| \frac{M_\gamma(482)}{M_\gamma(343)} \right|$$

$$\sim \frac{200}{50} = 4 \pm 2.$$

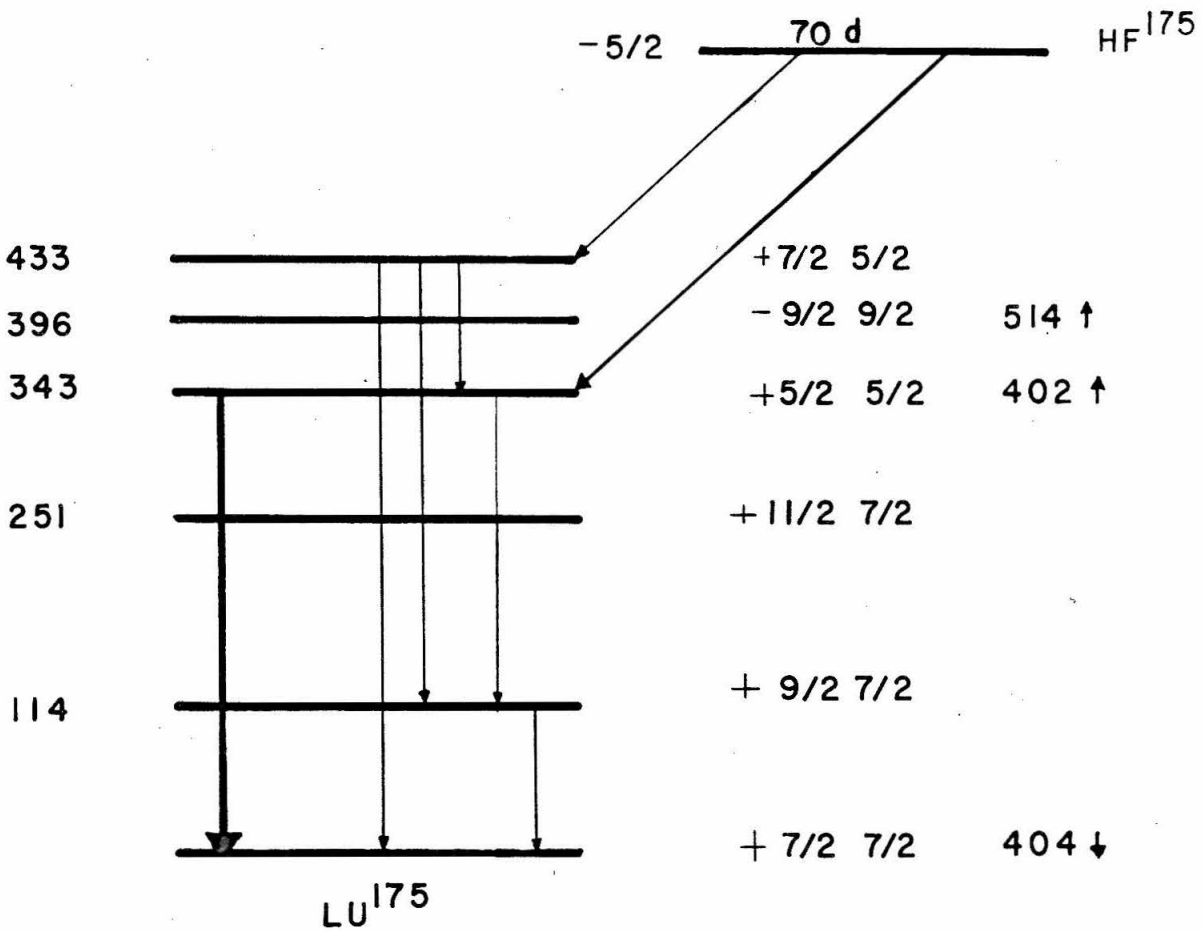

Fig. 9

Level Scheme of Lu^{175}

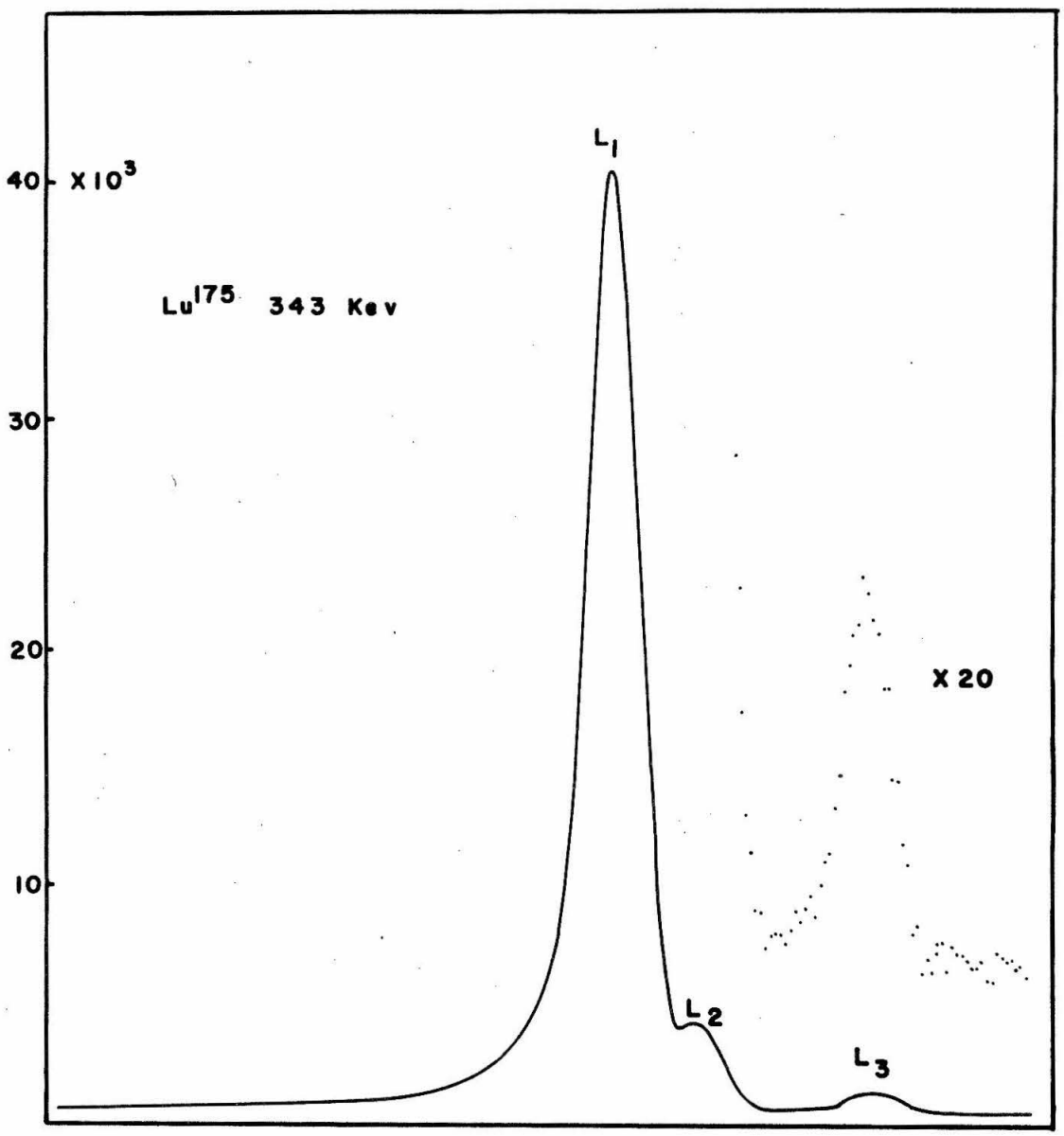

Fig. 10

L-Shell Internal Conversion Spectrum of the 343 keV Line in Lu^{175}

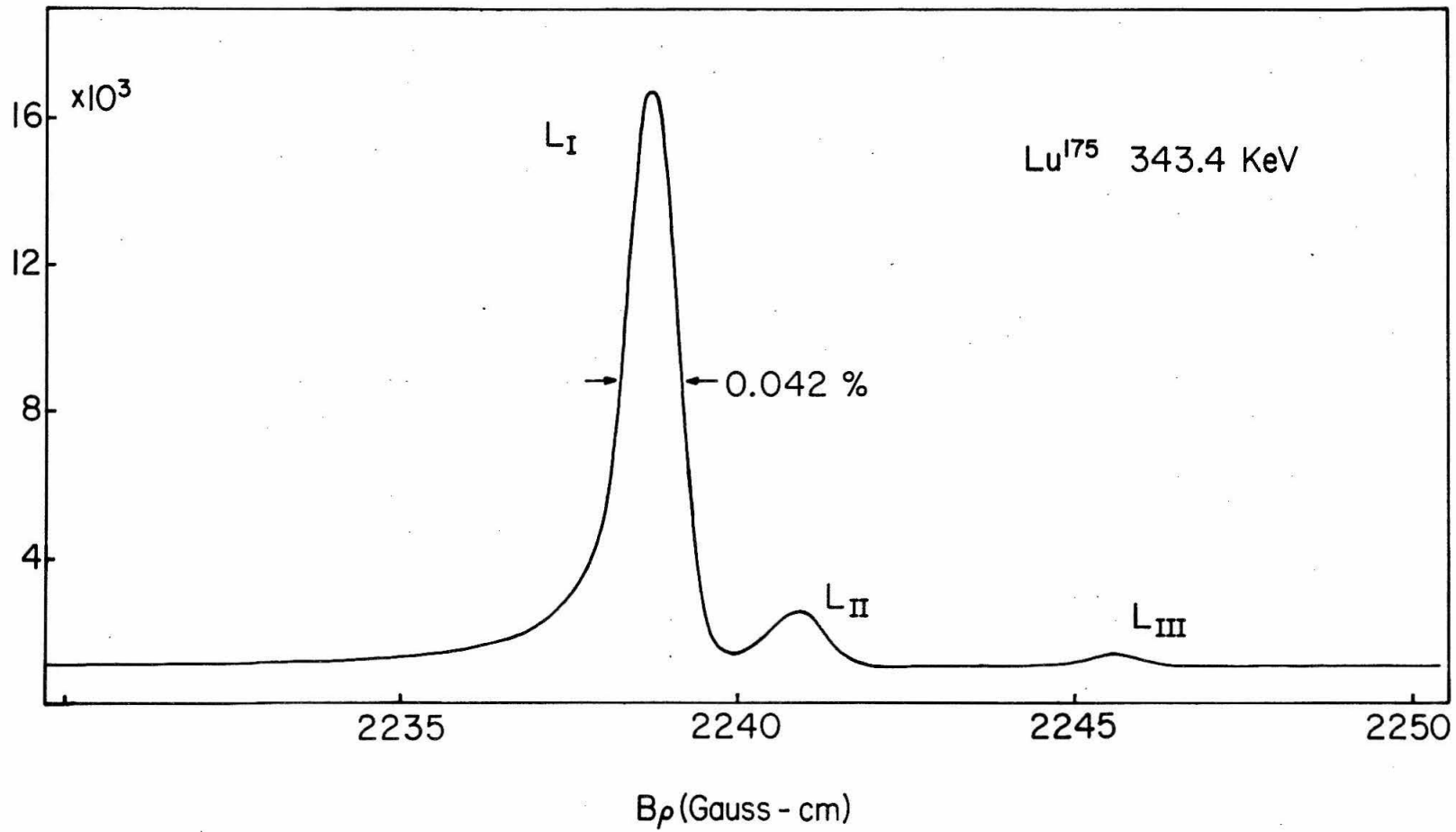

Fig. 11

L-Shell Internal Conversion Spectrum of the 343 keV Line in Lu^{175}

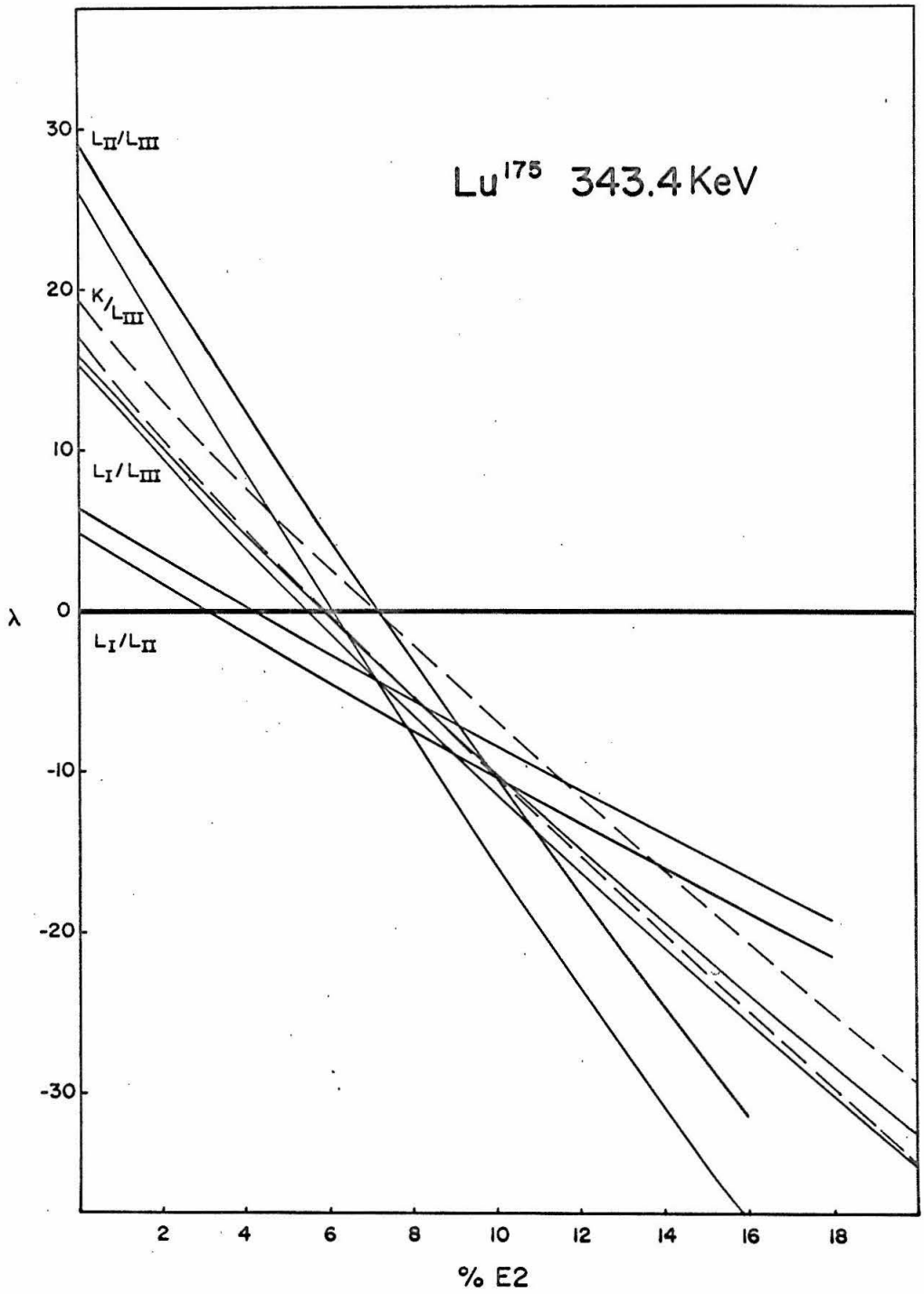

Fig. 12

Variation of λ vs percentage E2
Lines represent limits due to experimental errors

This value of λ is in good agreement with the experiments, which show the possibility of $|\lambda|$ being this large.

B. Comparison of Results with Nuclear Model Calculations

In order to test our understanding of the nuclear wave functions, one can calculate the various matrix elements that have been experimentally measured. They are, the magnetic moments of the excited and ground states, the electric quadrupole and magnetic dipole transition widths and now the penetration matrix element. In Table 3, we give the various contributions to the intrinsic magnetic dipole g-factor. We use an effective spin g-factor, g_s^{eff}, in order to represent the quenching of the spin contribution due to core polarization. This quenching is a characteristic feature of the magnetic moments of all nuclei and has been extensively discussed recently by Bodenstedt and Rogers[64] and Nilsson[65]. If we then sum the contributions due to the convection current, spin current and the spin-orbit induced current (which is small), we find good agreement with experiment. The contribution to the magnetic moment due to the $\vec{L}\cdot\vec{L}$ term which is customarily included in the single particle Hamiltonian is unreasonably large. This term is introduced in order to represent the effect of the lowering of higher orbital angular momentum states in a square well. The nuclear potential is closer to a square well for heavy nuclei than the harmonic oscillator potential used. These $\vec{L}\cdot\vec{L}$ contributions should probably be neglected because it is apparent that the inclusion of such phenomenological terms is unsatisfactory from the point of view of calculating electromagnetic moments. The same problems

	ORIGIN	INTRINSIC g-FACTOR	
404↓	$\frac{\overline{I}+g_s^{eff}\ \overline{\sigma}}{k}$	+ .69	g_s^{eff} = .6 × 2.79
	Expt.	+ .7	(g_R = .4) Ref. (71)
	$\overline{I}\cdot\overline{s}$	− .05	
	$\overline{I}\cdot\overline{I}$	− .60	
402↑	$\frac{\overline{I}+g_s^{eff}\ \overline{\sigma}}{k}$	1.43	g_s^{eff} = .6 × 2.79
		1.84	" = 1. × 2.79
	Expt.	+ 1.75	(g_R = .4) Ref. (64)
	$\overline{I}\cdot\overline{I}$	+ .4	

Table 3

Contributions to magnetic g - factors for the 402↑ and 404↓ levels in Ta^{181}

arise when the effect of tensor forces is simulated by the spin-orbit potential. To neglect the contributions originating from these terms, as is almost always done, is not consistent either, since the wave functions reflect the existence of these terms in the Hamiltonian. We shall neglect the $\vec{L}\cdot\vec{L}$ term completely and estimate the effect of the $\vec{L}\cdot\vec{s}$ term.

The M1 gamma-ray amplitude is especially interesting as it is highly retarded in Ta^{181} and not nearly so retarded in Lu^{175}. In Table 4 we give the various contributions to the M1 rate. In the first section of Table 4, we compare the results of calculations of the M1 rate with the experimental values in the two cases. A contribution due to bandmixing results from the possibility that the two bands, $[402]\uparrow$ and $[404]\downarrow$, may be mixed by means of the Coriolis interaction. The interaction operator, $I_+J_- + I_-J_+$, is asymptotically hindered though. The calculated amplitude of the I = 7/2, K = 5/2 impurity in the I = 7/2, K = 7/2 level is roughly 4% for Ta^{181} and somewhat more for Lu^{175}. These estimates should be accurate to within a factor of two. The interesting thing is that the M1 amplitude due to the impurity is of the correct order of magnitude and sign to cancel the direct term in Ta^{181}. Then as the bands are closer in Lu^{175} and the mixing correspondingly increased; the M1 rate may increase. While this is an attractive explanation for the peculiar variation in the measured M1 rates for this transition, it is contradicted by two facts. First, the penetration amplitude is allowed and its amplitude can be calculated reasonably accurately. (See middle

	Origin	$(f\|\|-\|\|i)^{\dagger}$
$M1_{\gamma}$	$\bar{T}+2.79\cdot.6\cdot\bar{\sigma}$	-2.
	$\bar{T}\cdot\bar{s}$	+.51
	402↑ Coriolis impurity — (-.04) amplitude	+.32
	expt. Lu^{175}	±.25
	" Ta^{181}	$+1.8\times10^{-3}$
$M1_{Pen.}$	$g_s^{eff}(2r^2\bar{\sigma}-\bar{\sigma}\cdot\bar{r}\bar{r})$	+ 410 if $(\|\|M1_{\gamma}\|\|)>0$
	$r^2\bar{T}$	-96 " "
		Σ +320
	expt. λ Ta^{181}	+175
$E2_{\gamma}$	$E2_{\gamma}$ expt. Ta^{181}	$+3.1\times10^{-5}$
	" " Lu^{175}	$\pm5.\times10^{-5}$
	theo.:	
	402↑ → 404↓	-3.4×10^{-6} *
	-.04 402↑ in 404↓	$+1.8\times10^{-4}$ **
	+.01 402↓ in 402↑	-1.1×10^{-5} *

† arbitrary units
*reduced further by factor: $(u_i u_f - v_i v_f)^2$
**not affected by pairing correlations

Table 4

Comparison of Experimental Values with Theoretical Estimates of Reduced Matrix Elements

section , Table 4.) Therefore, its phase can be calculated, and is, in fact, positive. Since the ratio of the penetration amplitude to the normal M1 amplitude, λ, is positive for Ta^{181}, we can deduce that the phase of the normal M1 amplitude is positive also. As the band mixing impurity makes a contribution that is positive and is expected to increase in Lu^{175}, we should expect the λ in Lu^{175} to be positive. The evidence we have indicates that it is negative. The data for the Lu^{175} case can perhaps be understood in terms of anomalies in the E2 L shell conversion. We will discuss the problem of discrepancies in E2 L shell conversion in the next section. In any case, there is enough uncertainty in the experimental determination of the λ in the 343 KeV transition in Lu^{175} to reject it as an argument against the bandmixing solution of the M1 rate problem.

A second problem for the bandmixing explanation is the retarded E2 rates. The direct E2 amplitude between the bands is asymptotically hindered, but the K-impurity gives rise to a collectively enhanced amplitude that is many times the measured rate. In the third section of Table 4, we see that the $[402]\uparrow 5/2$ impurity in the $[404]\downarrow 7/2$ state makes a collective contribution to the E2 transition amplitude that is 4-6 times the measured rate. Another level that may contribute is the $[402]\downarrow 3/2$ admixture in the $[402]\uparrow 5/2$ level. The E2 amplitudes that result from the admixture of the other bands are not collective and will be retarded by the pairing correlation factor, $(U_i U_f - V_i V_f)$. If the M1 amplitude due to bandmixing is large enough to cancel the direct M1 amplitude, then the E2 rate is much too large.

The E2 amplitude due to impurities admixed by the Coriolis force is too large by a factor 6 in Ta^{181} and 4 in Lu^{175}. The Coriolis operator $J_+ = \ell_+ + s_+$ being similar to the M1 operator, $g_L\ell_+ + g_s s_+$ may also be excessively retarded for the case of the $[402]\uparrow$ band mixing with the $[404]\downarrow$ band.

The size of the calculated penetration amplitude is in good agreement with experiment considering that we do not know what effect core polarization may have for non-diagonal M1 matrix elements. This agreement allows us to assume that we can correctly calculate the penetration matrix element, including its sign. Knowing the sign of the penetration matrix element, as well as the experimental λ, yields a determination of the sign of the M1 gamma-ray transition amplitude. The parity experiment of Boehm and Kankeleit detects an interference between the M1 amplitude and the E1 parity impurity amplitude. Having the sign of the M1 amplitude is essential before one can compare the measured E1 amplitude with theoretical predictions.

Also, knowing the M1 phase and the phase of the M1 - E2 interference term, $\delta = +6.4$[56], we find that the E2 transition amplitude is positive. This is in agreement with the prediction that the band mixing impurity in Ta^{181} is dominant and has positive phase, The direct single-particle amplitude is negative.

C. Anomalies in Electric Quadrupole Internal Conversion in the L Shell

In recent years there has been considerable interest in E2 internal conversion. It was precipitated by Mcgowan and Stelson, who reported that a number of $2^+ \rightarrow 0^+$ transitions had K conversion

coefficients that were up to 20% higher than the theoretical conversion coefficients[66]. Subba Rao[67] has tried to show a dependence of the deviation on A, the atomic weight. There appeared to be larger deviations from the theoretical coefficients in the region of deformed nuclei. Listengarten, reviewing the situation in 1962, found that the deviation could be attributed to difficulties with the various experimental techniques used[20]. These difficulties were at that time either being overcome or at least understood. The deformed nuclei with their low-lying 2^+ states were especially vulnerable to experimental uncertainties such as the photoelectric angular distribution which must be known in the external-internal conversion method. Since in a few cases the experimental conversion coefficients were approaching 1% agreement with the theoretical values, it seemed that there was no problem with E2 conversion. In 1964 M. Mladjenovic voiced concern about E2 conversion in the L shell[68]. L subshell ratios can be measured with a much greater precision than absolute conversion coefficients.

In the series of nuclei that we examined for penetration effects, there occurred three E2 transitions that are good candidates for a 1-2% measurement of the L subshell ratios. They are the 100 keV $2^+ \rightarrow 0^+$ intraband transition in W^{182}, the 130 keV $7/2^+ \rightarrow 3/2^+$ intraband transition in Tm^{169}, and the 133 keV $1/2^+ \rightarrow 5/2^+$ interband transition in Ta^{181}. The first two transitions are enhanced collective transitions with rates over one hundred times that of single particle estimates. The third transition is a hindered interband transition which is retarded by a factor of over 200 from the single particle

Weisskopf estimate.

The sources were prepared by evaporation as fluorides as was discussed in the experimental technique section. High resolution and very thin sources are required. This may seem surprising since the cases are at relatively low energy and should be easily resolved. However, internal conversion in the L shell has the following pattern at low energies: the L_{II} and L_{III} shells have approximately the same intensities, while the L_I shell is 10 times weaker in intensity. The L_I line then lies on top of the "tail" of the nearby L_{II}. The background must be measured over a range above and below the L shell lines. To analyze the data, the background is subtracted and then the data are plotted on semi-logarithmic paper. Since the line shapes are the same for all three lines, the isolated L_{III} line serves as a model of the line shape. By iteration the L_I and L_{II} lines may be resolved. Then, either the resolved peak heights or the areas weighted by the known change in momentum acceptance of the spectrometer serve as a measure of the L subshell intensities. We find the L_{II}/L_{III} ratio to within 1% in these cases, and the L_I/L_{III} or L_I/L_{II} ratios are accurate to 2 to 4%. Figures 13, 14, and 15 show the L shell spectra. In Table 5 we give the L subshell ratios, as well as the theoretical ratios of Sliv, Rose, and the theoretical values we calculated.

The general trend is for the experimental L_I/L_{II} ratio to be about 10% higher than the theoretical ratio. The L_{II}/L_{III} ratio is consistently about 3% lower than theory. These trends were also

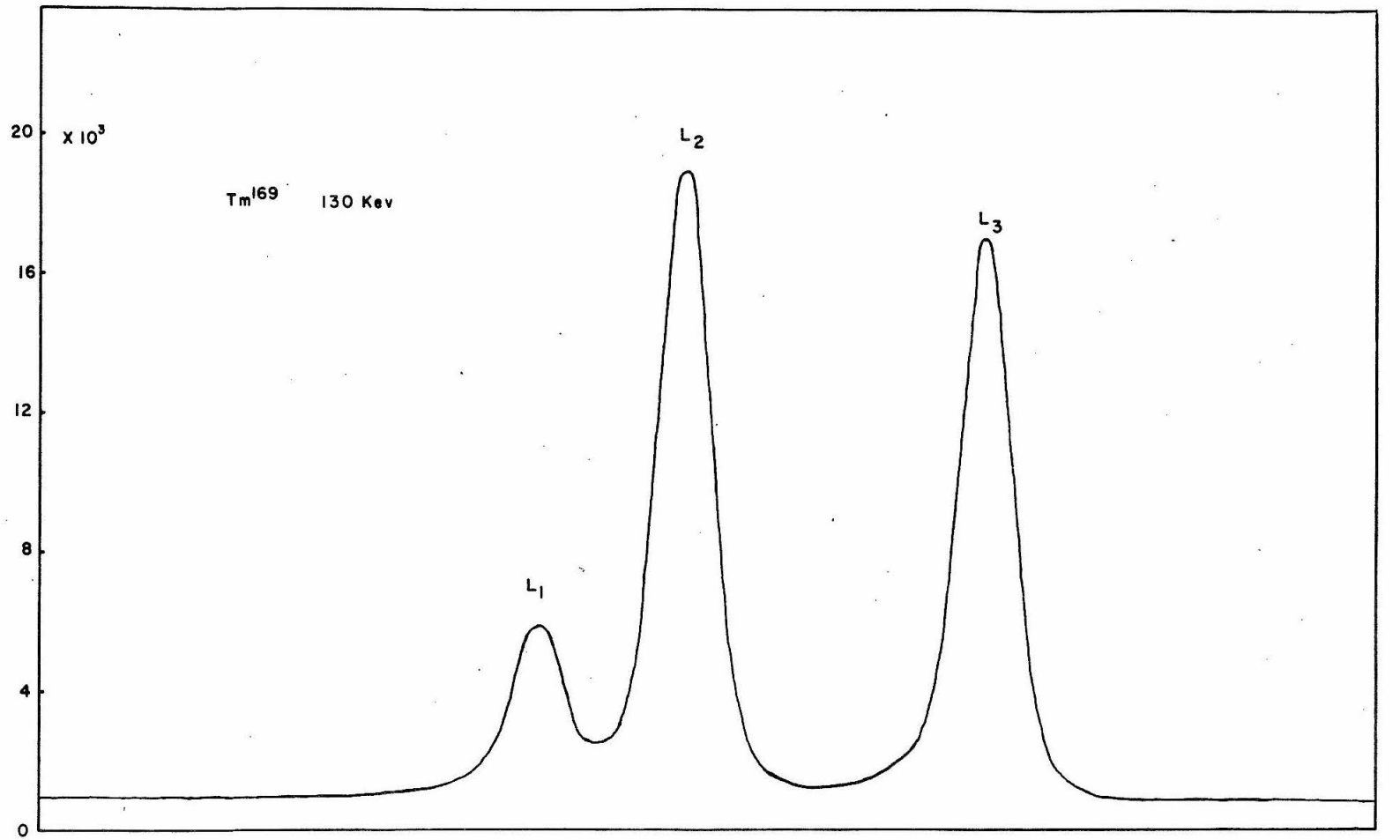

Fig. 13

L-Shell Internal Conversion Spectrum for the 130 keV Line in Tm^{169}

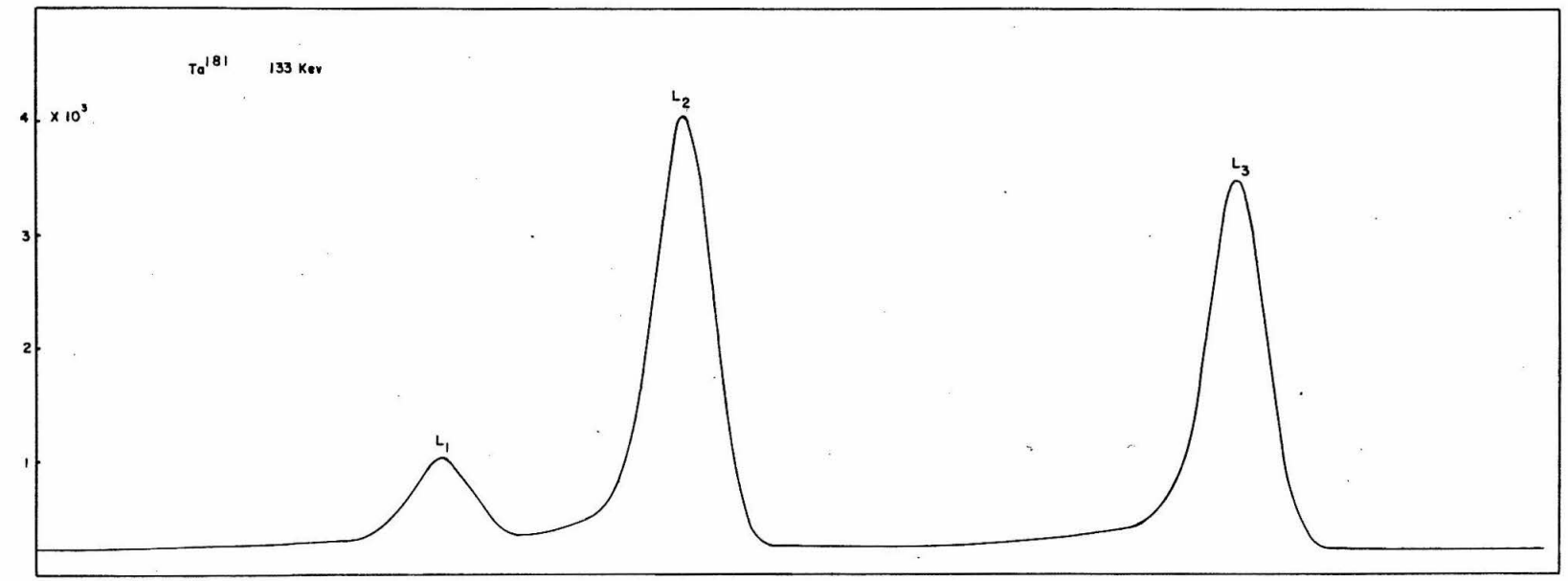

Fig. 14

L-Shell Internal Conversion Spectrum for the 133 keV Line in Ta^{181}

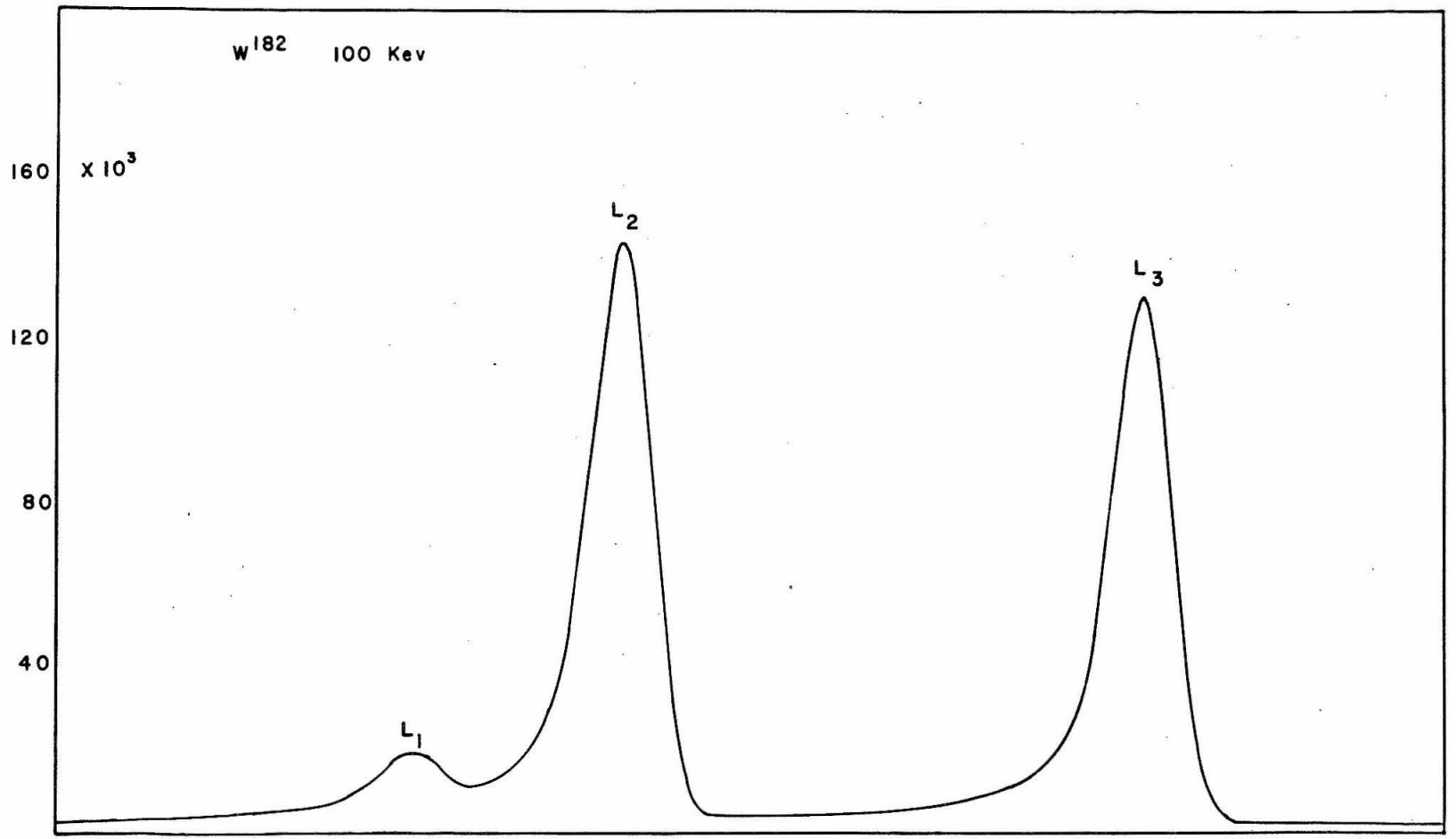

Fig. 15

L-Shell Internal Conversion Spectra for the 100 keV Line in W^{181}

		L1/L2	L1/L3	L2/L3
Tm^{169}	130.5 KeV			
	Expt.	.254 ± .005	.280 ± .006	1.10 ± .01
	Rose	.242	.265	1.12
	Sliv	.242	.278	1.16
	C.I.T.	.237	.272	1.14
Te^{181}	133.0 KeV			
	Expt.	.190 ± .006	.223 ± .006	1.18 ± .02
	Rose	.173	.203	1.17
	Sliv	.174	.211	1.20
	C.I.T.	.173	.211	1.22
W^{182}	100.0 Kev			
	Expt.	.095 ± .004	.104 ± .004	1.09 ± .01
	Rose	.083	.090	1.09
	Sliv	.081	.090	1.12
	C.I.T.	.081	.091	1.12

Table 5

L-Subshell Ratios, Experimental and Theoretical

reported recently for many nuclei in the deformed region by M. Mladjenovic et al., at the International Conference on the Internal Conversion Process[69], though with somewhat less precision than the results presented here. While they reported the anomaly in the L_I/L_{II} ratio, they found the L_{II}/L_{III} to be normal within their precision.

D. Estimation of Penetration Effects

In an attempt to explain these anomalies in E2 L shell conversion, it is reasonable to look for penetration effects, but since the E2 transitions in W^{182} and Tm^{169} are enhanced collective transitions, penetration effects are not expected to be important. The $\lambda(j\cdot\nabla)$ ratio (Table 1), turns out to be approximately unity. The calculation of this collective penetration matrix element chould be as accurate as for the normal collective quadrupole matrix element. Bes and Szymanski have obtained excellent agreement with experiment for intrinsic quadrupole moments[70]. Our calculations, while less elaborate, give essentially the same results for the intrinsic quadrupole moment, and presumably, therefore, an accurate estimate of the $j\cdot\nabla$ penetration matrix element. The $j\cdot r$ penetration matrix element, while weighted approximately 10 times less than the $j\cdot\nabla$ type, is enhanced by the $\omega_K \sim 50$ - 80 factor. However, in the case of collective transitions, the $j\cdot r$ matrix element, actually an expectation value for the intrinsic state, vanishes identically for both the spin and convection currents. To summarize, it appears that a $\lambda(j\cdot\nabla) \sim 1$ is all that can be attributed to penetration. This value of λ changes the L shell E2 conversion coefficients by less than 1%.

Taking the theoretical formulae for the L subshell ratios, including the perturbation amplitudes, one finds that there are no values of $\lambda(j\cdot\nabla)$ and $\lambda(j\cdot r)$ which satisfy the experimental data. This agrees with the conclusions based on the theoretical estimates of the λ's.

The 133 keV transition in Ta^{181} is a hindered single-particle transition that might be expected to show penetration effects. The $j\cdot\nabla$ matrix element gives rise to a $\lambda(j\cdot\nabla)$ that is of the order of unity and therefore unimportant. This is so because the single-particle Nilsson estimate for the E2 gamma transition amplitude agrees with experiment before pairing corrections are made. These corrections should reduce the transition amplitude by perhaps a factor of 5. That the E2 rate is faster than estimated is evidence of significant Coriolis impurities in the $[411]\downarrow$ and $[402]\uparrow$ bands involved. The $j\cdot\nabla$ penetration matrix element of either the collective admixture or the direct contribution gives a $\lambda(j\cdot\nabla)$ which is less than unity. The $\lambda(j\cdot r)$ derived from the spin current on the other hand is estimated to be as large as 150. The pairing corrections for the $j\cdot r$ matrix elements are not important because they change sign under time reversal. A $\lambda(j\cdot r)$ of this size changes the conversion coefficients appreciably:

$$\lambda = \pm 150$$

$$L_I : \begin{matrix} +6 \\ -1 \end{matrix} \%$$

$$L_{II} : \begin{matrix} + \\ - \end{matrix} 9 \%$$

$$L_{III} : \begin{matrix} - \\ + \end{matrix} 5 \%$$

These changes do not agree with the data. Also in this case there is no set of λ's which is consistent with the data. The fact that the L shell anomalies in this retarded transition are identical to those in the enhanced W^{182} and Tm^{169} transitions suggests that the estimated $\lambda(j\cdot r) \sim 150$ is too large at least by a factor of 5. This discrepancy with experiment can perhaps be attributed to the uncertainty in estimating the spin quenching.

E. Other Possible Causes of the E2 Anomalies

We have investigated the possibility that the nuclear quadrupole perturbs the bound state wave function. This is the Sternheimer shielding effect[73]. For s-states, the Schrödinger Equation was solved for coupled s and d states. The d wave admixture was too small by several orders of magnitude to have any significant effect on the conversion coefficients.

The effect of higher order processes on internal conversion has been considered by Krutov[74,75]. He did not include positron intermediate states. The diagrams that should be considered are shown in Fig.16 . The first diagram gives the amplitude for internal conversion that is usually considered. The last two diagrams give the higher order corrections to the first diagram. They can be reduced to integrals over the electron radial variable, but just as with the penetration amplitude, the integration over the two-electron wave function cannot be written as the product of two integrals. This prevents us from using our program to calculate these corrections. It will not be too difficult to modify it in the future to do these

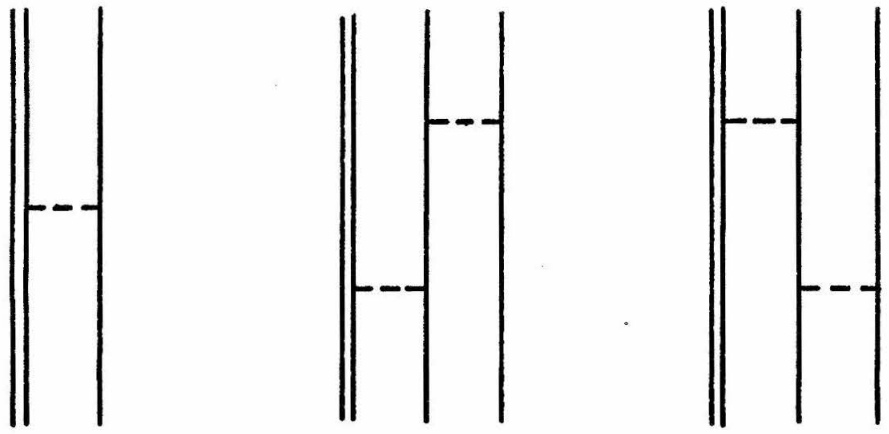

Fig. 16

Lowest Order Contribution to Internal Conversion together with Higher Order Corrections.

integrals. These corrections have never been estimated, so even if they do not explain the E2 anomalies they will be of interest.

CONCLUSIONS

We have described calculations of conversion coefficients, incorporating several improvements over previous calculations. Our results show that the tabulated values of Sliv and Band are preferable to those of Rose, although at the extremes of high and low energy and high atomic number there are also discrepancies between our results and Sliv's. These may only partially be attributed to the fact that Sliv includes an estimate for penetration effects. Our programs may be extended in order to calculate particle parameters for the analysis of gamma-conversion electron (polarized or unpolarized) directional correlations, which are being performed increasingly in recent years. As a by-product of these calculations we get the electron wavefunctions at the nucleus which are useful for the analysis of beta decay and electron capture experiments. The programs could easily be generalized for the calculation of other processes: K and L photoelectric absorption (the former has not been calculated using screened and finite nuclear size wavefunction and the latter has never been calculated relativistically), Mott scattering; internal bremsstrahlung and internal pair formation. The last two processes have never been calculated with atomic wavefunctions. Nuclear size effects could be important. Photoelectric absorption and Mott scattering have been used in recent years in order to analyze decay radiations in low energy nuclear physics experiments.

We have seen that one might expect penetration effects to be important in internal conversion, if the normal transition amplitude is sufficiently

retarded. However, if the penetration amplitude is retarded also or if the transition is K-forbidden then penetration effects are less probable. We have seen that if the gamma-ray amplitude is retarded, the greater complexity of the penetration operator often causes it to be allowed. In the case of electric transitions the dominant penetration amplitude has time-reversal properties which prevent the cancellation due to pairing correlations that occur for the normal electric amplitude in single-particle transitions.

The care required in making internal conversion measurements with a magnetic spectrometer has been discussed. The experiments concerning the analogous retarded M1 transitions in Ta^{181} (482 keV) and Lu^{175} (343 keV) showed a $\lambda = +175$ in Ta^{181} and the possibility of a λ in Lu^{175} that is consistent with the result for Ta^{181}, considering that the states are analogous. Estimation of the penetration amplitude from nuclear model considerations, gives reasonable results. The estimated penetration amplitude is within a factor of two of the experimental amplitude. The M1 and E2 amplitudes are not in as good agreement however. The effect of spin quenching, which is seen in magnetic dipole moments, should be investigated for M1 transition amplitudes.

High precision L subshell measurements of low energy E2 transitions in W^{182}, Tm^{169}, and Hf^{181} show that the L1/L2 ratio is systematically 5 - 15% higher than the theoretical calculations predicted. The L2/L3 ratio may be systematically low by roughly 3%. Investigation of possible penetration effects show that they cannot

explain the data. Theoretical estimates indicate that one should not expect penetration effects in W^{182} and Tm^{169}. Unreasonably large penetration effects are predicted for the 133 keV transition in Ta^{181}. The predicted E2 penetration amplitude is almost entirely derived from the spin current, indicating again that spin quenching effects may be the trouble. The possibility of higher order corrections should be investigated as a possible explanation of the E2 anomalies. If the higher order corrections are significant, then they presumably will be present in the internal conversion of other multipole radiation.

APPENDIX I.

We are interested in solutions of the Dirac Equation for a central field. We will summarize here various formulae that are useful in problems concerning an electron in a central field. The standard text on electron theory by Rose[38] serves as a reference.

The Dirac Equation has solutions for a central potential which are eigenfunctions of the total angular momentum.

$$\psi_\kappa^\mu = \begin{pmatrix} -i f_\kappa(r)\, \chi_{-\kappa}^\mu \\ g_\kappa(r)\, \chi_\kappa^\mu \end{pmatrix} . \tag{49}$$

The two component spinor χ_κ^μ is given by

$$\chi_\kappa^\mu = \sum_m (L\, \tfrac{1}{2}\, j;\, m,\, \mu-m)\, Y_L^m\, \chi^{\mu-m} \tag{50}$$

where $\chi^{\mu-m}$ is a Pauli spinor and j and L are determined by κ:

$$(\sigma \cdot L + 1)\, \chi_\kappa^\mu = -\kappa\, \chi_\kappa^\mu . \tag{51}$$

The equation defining κ leads directly to

$$\begin{aligned} j &= \ell + 1/2 : \quad \kappa = -(\ell + 1) \\ j &= \ell - 1/2 : \quad \kappa = \ell, \end{aligned} \tag{52}$$

or

$$j = s_{1/2}, p_{3/2}, d_{5/2}, f_{7/2}, \ldots$$

for

$$\kappa = -1, -2, -3, -4, \ldots$$

and

$$j = p_{1/2},\ d_{3/2},\ f_{5/2},\ \cdots$$

for

$$\kappa = +1, +2, +3, \ldots .$$

Now, with κ so defined, we may write the first order radial equations.

$$\begin{aligned} \frac{dg_\kappa}{dr} &= -\frac{\kappa+1}{r} g_\kappa + (W - V + 1) f_\kappa \\ \frac{df_\kappa}{dr} &= -(W - V - 1) g_\kappa + \frac{\kappa - 1}{r} f_\kappa . \end{aligned} \tag{53}$$

The reduced radial function

$$g_\kappa \to r\, g_\kappa,\ f_\kappa \to r\, f_\kappa$$

is useful. Their equations are

$$\begin{aligned} \frac{dg_\kappa}{dr} &= -\frac{\kappa}{r} g_\kappa + (W + 1 - V) f_\kappa \\ \frac{df_\kappa}{dr} &= -(W - 1 - V) g_\kappa + \frac{\kappa}{r} f_\kappa . \end{aligned} \tag{54}$$

Some useful relations for reducing matrix elements involving wave functions of the Dirac Equation are

$$\sigma_r \chi^\mu_\kappa = -\chi^\mu_{-\kappa} \tag{55}$$

with

$$\sigma_r = \vec{\sigma}\cdot\vec{r}/r.$$

$$\vec{\alpha}\cdot\vec{\nabla} = \rho_1 \, \sigma_r \left(\frac{\partial}{\partial r} + \frac{1}{r}\right) - \frac{1}{r} \rho_1 \, \sigma_r (\vec{\sigma}\cdot\vec{L} + 1) \tag{56}$$

with

$$\vec{\alpha} = \begin{pmatrix} 0 & \vec{\sigma} \\ \vec{\sigma} & 0 \end{pmatrix} \quad \text{and} \quad \rho_1 = \begin{pmatrix} 0 & 1 \\ 1 & 0 \end{pmatrix}$$

and

$$r \, \vec{\sigma}\cdot\vec{\nabla} = \sigma_r \left(r \frac{\partial}{\partial r} - \vec{\sigma}\cdot\vec{L}\right). \tag{57}$$

APPENDIX II

Rather than use the definition of the multipole potentials in terms of vector spherical harmonics as in Eq. (3), we shall define them in terms of vector operators:

$$\vec{A}_L^m(M) = \frac{\vec{L}\, j_L(Kr)\, Y_L^m}{\sqrt{L(L+1)}}$$

$$\vec{A}_L^m(e) = \frac{1}{K\sqrt{L(L+1)}} \left\{ \vec{\nabla} \frac{d}{dr} + K^2 \vec{r} \right\} r\, j_L(Kr)\, Y_L^m \qquad (58)$$

$$\vec{A}_L^m(\ell) = \frac{\vec{\nabla}\, j_L(Kr)\, Y_L^m}{k} \quad .$$

In order to derive Eq. (7) from Eq. (6) we must do the angular integrals,

$$\int \vec{j}_e \cdot \vec{B}_L^m(M) \sim \int \psi_f^* \vec{\alpha} \cdot (\vec{L}\, h_L(Kr)\, Y_L^m)\, \psi_i \,. \qquad (59)$$

Now, using

$$\int j \cdot B \sim \int \begin{pmatrix} -i\, f_{\kappa_f} \chi^{\mu_f}_{-\kappa_f} \\ g_{\kappa_f} \chi^{\mu_f}_{\kappa_f} \end{pmatrix}^* \rho_1\, \vec{\sigma} \cdot (\vec{L}\, h_L(Kr)\, Y_L^m) \begin{pmatrix} -i\, f_{\kappa_i} \chi^{\mu_i}_{-\kappa_i} \\ g_{\kappa_i} \chi^{\mu_i}_{\kappa_i} \end{pmatrix}$$

$$= \int \begin{pmatrix} -i\, f_{\kappa_f} \chi^{\mu_f}_{-\kappa_f} \\ g_{\kappa_f} \chi^{\mu_f}_{\kappa_f} \end{pmatrix}^* \rho_1 \left\{ \vec{\sigma} \cdot \vec{L} (L_L Y_L^m) - h_L Y_L^m\, \vec{\sigma} \cdot \vec{L} \right\} \begin{pmatrix} -i\, f_{\kappa_i} \chi^{\mu_i}_{-\kappa_i} \\ g_{\kappa_i} \chi^{\mu_i}_{\kappa_i} \end{pmatrix} \qquad (60)$$

$$= i\int (g_{\kappa_f} f_{\kappa_i})\, h_L\, dr^{*}(\kappa_f + \kappa_i)\ (\kappa_f\ \mu_f|Y_L^m|-\kappa_i\ \mu_i)$$

$$+ i\int (f_{\kappa_f} g_{\kappa_i})\, h_L\, dr\cdot(\kappa_f + \kappa_i)\ (-\kappa_f\ \mu_f|Y_L^m|\ \kappa_i\ \mu_i). \tag{60}$$

With Eq. (55) we can show the second angular integral is equal to the first.

$$\int j\cdot B \backsim i\ (\kappa_f\ \mu_f|Y_L^m|-\kappa_i\ \mu_i)(\kappa_f+\kappa_i)\int (g_{\kappa_f} f_{\kappa_i} + f_{\kappa_f} g_{\kappa_i})h_L\, dr\ . \tag{61}$$

The angular integral is performed using Eq. (50) and recoupling angular eigenfunctions in the usual way. All other angular integrations in Eq. (6) are identical to this one.

The reduction of Eq. (5) is somewhat lengthier. First we will state that by introducing Eq. (58) for the longitudinal potential and doing the partial integrations, the longitudinal contribution is found to exactly cancel the scalar potential contribution except for a surface term which is canceled by an identical term which arises in the electric amplitude. The remaining terms in Eq. (5) are reduced by using Eq. (58) for the definition of the $\vec{A}_L^m(e)$. One then finds two types of electron angular integrals: $\vec{\alpha}\cdot\vec{\nabla}$ and $\vec{\alpha}\cdot\vec{r}$. Using Eqs. (55) and (56) we may proceed just as in the magnetic case. The electron radial integrals for the electric case are

$$\int_0^\infty \left[(g_{\kappa_f} f_{\kappa_i} - f_{\kappa_f} g_{\kappa_i})k - (g_{\kappa_f} g_{\kappa_i} + f_{\kappa_f} f_{\kappa_i})\frac{d}{dr}\right]\ r\, h_L\, dr\ .$$

The penetration terms are of the form,

$$\int \vec{j}_n \cdot \vec{\nabla} \; \Phi \; (r) \; Y_L^m$$

and

$$\int \vec{j}_n \cdot \hat{r} \;\; \theta \; (r) \; Y_L^m$$

where, (the primed wavefunctions belong to the initial state),

$$\theta = - \frac{i}{k} (gf' - fg') + r \, h_L \int_0^r \left[k^2 (gf' - fg') - k(gg' + ff') \frac{d}{dr} \right] r \, j_L$$
$$- r \, j_L \int_0^r \left[K^2 (gf' - fg') - K(gg' + ff') \frac{d}{dr} \right] r \, h_L , \tag{62}$$

and

$$\Phi = - \frac{d}{dr} (r \, h_L) \left[\int_0^r K(gg' + ff') \frac{d}{dr} (r \, j_L) \right.$$
$$\left. - K^2 \int_0^r r \, j_L \, (gf' - fg') \right]$$
$$+ \frac{d}{dr} (r \, j_L) \left[\int_0^r K(gg' + ff') \frac{d}{dr} (r \, h_L) \right. \tag{63}$$
$$\left. - K^2 \int_0^r r \, h_L (gf' - fg') \right] \quad .$$

REFERENCES

1. R. Wilson, "Alpha, Beta, and Gamma-Ray Spectroscopy" Vol. 2, 1557 (North-Holland Publishing Company, Amsterdam, 1965).

2. E.L. Church and J. Weneser, Phys. Rev. 100, 943, 1241(A) (1955).

3. E.L. Church and J. Weneser, Phys. Rev. 104, 1382 (1956).

4. B. Swirles, Proc. Roy. Soc.(London), A121, 447 (1928).

5. H.B. Casimir, Nature 126, 953 (1930).

6. R.H. Fowler, Proc. Roy. Soc.(London), A129, 1 (1930).

7. H.R. Hulme, Proc. Roy. Soc.(London), A138, 643 (1932).

8. H.M. Taylor and N.F. Mott, Proc. Roy. Soc.(London), A138, 665 (1932); A142, 215 (1933).

9. J.B. Fisk, Proc. Roy. Soc.(London), A143, 674 (1933).

10. J.B. Fisk and H.M. Taylor, Proc. Roy. Soc.(London), A146, 178 (1934).

11. M.E. Rose, G.H. Goertzel, B.I. Spinrad, J. Harr, and P. Strong, Phys. Rev. 83, 79 (1951).

12. M.E. Rose, G.H. Goertzel and C.L. Perry, ORNL Report No. 1023.

13. J.R. Reitz, Phys. Rev. 77, 10 (1950).

14. L.A. Sliv, J.E.T.P. 21, 770 (1951).

15. L.A. Sliv and M.A. Listengarten, J.E.T.P. 22, 29 (1952).

16. L.A. Sliv and I.M. Band, Report 57 ICC K1, (K shell). Report 58 ICC L1, (L shell), Physics Department, University of Illinois.

17. M.E. Rose, "Internal Conversion Coefficients" (North-Holland Publishing Company, Amsterdam, 1958.

18. T.A. Green and M.E. Rose, Phys. Rev. 110, 105 (1958).

19. M.A. Listengarten, Bull. Acad. Sci. U.S.S.R., Phys. Ser. (Engl. Transl.) 22, 759 (1958).

20. M.A. Listengarten, Bull. Acad. Sci. U.S.S.R., Phys. Ser. (Engl. Transl.) 26, 1479 (1962).

21. T. Novakov and J.M. Hollander, Nuclear Phys. 60, 593 (1964).

22. C. Moller, Ann. Physik, 14, 531 (1932).

23. M.E. Rose "Multipole Fields". (Wiley, New York, 1955).

24. N. Tralli and G.H. Goertzel, Phys. Rev. 83, 399 (1951).

25. A.I. Akhiezer and V.B. Berestetskii "Quantum Electrodynamics". (Interscience, New York, 1965).

26. G. Kramer, Z. Physik, 146, 187 (1956); 147, 628 (1957).

27. K. Umeda, J. Fac. Sci. Hokkaido Imp. Univer. II, 3, 171 (1942).

28. M. Metropolis and J.R. Reitz, J. Chem. Phys. 19. 555 (1951).

29. L. Thomas, J. Chem. Phys. 22, 1759 (1954).

30. F. Herman and S. Skillman "Atomic Structure Calculations". (Prentice-Hall, New Jersey, 1963).

31. J.C. Slater, Phys. Rev. 81, 385 (1951).

32. J.C. Slater "Quantum Theory of Atomic Structure". Chap. 17, Vol. 2. (McGraw Hill Book Company, New York, 1960).

33. P.A.M. Dirac, Proc. Cambridge Phil. Soc. 26 376 (1930).

34. E. Wigner and F. Seitz, Phys. Rev. 43, 804 (1933).

35. R. Latter, Phys. Rev. 99, 510 (1955).

36. D. Liberman, J.T. Waber and D.T. Cromer, Phys. Rev. 137, A27 (1965).

37. P. Henrici "Discrete Variable Methods in Ordinary Differential Equations" (Wiley, New York, 1962).

38. M.E. Rose "Relativistic Electron Theory" (Wiley, New York, 1961).

39. R.H. Good, Phys. Rev. 90, 131 (1953).

40. G.T. Ewan and A.J. Tavendale, Can. J. Phys. 42, 2286 (1964).

41. C. Günther and H. Ryde, Private Communication.

42. J.W.M. DuMond, Technical Progress Reports C.I.T. Compton Spectrometer, I-VI, 1959-1963.

43. G.E. Lee-Whiting and E.A. Taylor, Chalk River Report CRT-668 (1956). (unpublished).

44. W.C. Parker and H. Slatis "Alpha, Beta, and Gamma-Ray Spectroscopy" Vol. 1., 379 (North-Holland Publishing Company, Amsterdam, 1965).

45. J.P. Elliot, Collective Motion in Nuclei, University of Rochester Report, NYO-2271 (1958).

46. O. Nathan and S.G. Nulsson, "Alpha, Beta, and Gamma-Ray Spectroscopy". Vol. 1, 601 (North-Holland Publishing Company, Amsterdam, 1965).

47. M.A. Preston "Physics of the Nucleus" (Addison-Wesley Publishing Company, Reading, 1962).

48. A.J. Rassey, Phys. Rev. 109, 949 (1958).

49. F. Asaro, F.S. Stephens, J.M. Hollander and I. Pearlman, Phys. Rev. 117, 492 (1960).

50. S.G. Nilsson and J. Rasmussen, Nuclear Phys. 5, 617 (1958).

51. E.L. Church and J. Weneser, Nuclear Phys. 28, 602 (1961).

52. G. Kramer and S.G. Nilsson, University of California Report UCRL-9877 (1961) unpublished.

53. L.S. Kisslinger and R.A. Sorensen, Matematiskfysiske Meddeleser, Det Kongelige Danske Videnskabernes Selskab, Bind 32, Nr. 9 (1960).

54. R. Hager, Ph.D. Thesis, California Institute of Technology, to be submitted, 1965.

55. E.L. Church and J. Weneser "Nuclear Structure Effects in Internal Conversion" Annual Review of Nuclear Science, Vol. 10 (1960).

56. Z. Grabowski, B.G. Petterson, T.R. Gerholm, and J.E. Thun, Nuclear Phys. 24, 251 (1961).

57. E.L. Church, A. Schwarzschild, and J. Weneser, Phys. Rev. 133, B 35 (1964).

58. L.C. Biedenharn and M.E. Rose, Phys. Rev. 134, B8 (1964).

59. F. Boehm and E. Kankeleit, Phys. Rev. Letters 14, No. 9 312 (1965).

60. P. Alexander, H. Ryde, and E. Seltzer, Proceedings of the International Conference on the Internal Conversion Process, Nashville 1965. Also to be published in Nuclear Phys.

61. T.R. Gerholm, B.G. Petterson and Z. Grabowski, Nuclear Phys. 65, 441 (1965).

62. Nuclear Data Sheets, National Academy of Sciences, National Research Council, 1960.

63. B.I. Deutch, Nuclear Phys. 30, 191 (1962).

64. E. Bodenstedt, and J.D. Rogers "Perturbed Angular Correlations". p. 91 (North-Holland Publishing Company, Amsterdam, 1964).

65. S.G. Nilsson "Perturbed Angular Correlations" p. 163 (North-Holland Publishing Company, Amsterdam, 1964).

66. F.K. McGowan and P.H. Stelson, Phys. Rev. 107, 1674 (1957).

67. B. Subba Rao, Nuovo Cimento, 17, 189 (1960).

68. M. Mladjenovic, Private Communication, 1964.

69. R. Stepic, M. Bogdanovic, and M. Mladjenovic. Oral Report, International Conference on the Internal Conversion Process, 1965, Nashville, Tennessee.

70. D. Bes, and Z. Szymanski, Nuclear Phys. 28, 42 (1961); M.Y.M. Hassan, Z. Skladanowski and Z. Szymanski, CALT-63-18 (1965).

71. L.H. Bennett and J.I. Budnick, Phys. Rev. 120, 1812 (1960).

72. E. Kankeleit, Rev. Sci. Instruments 35, 194 (1964).

73. R.M. Sternheimer, Phys. Rev. 84, 244 (1951).

74. V.A. Krutov, Izvest. Akad. Nauk SSSR, Ser. Fiz., No. 2 159 (1958).

75. V.A. Krutov and K. Muller, Izvest. Akad. Nauk SSSR, Ser. Fiz., No. 2 168 (1958).